processes

Article

Mathematical Modelling of the Entrainment Ratio of High Performance Supersonic Industrial Ejectors

Dario Friso

Department of Land, Environment, Agriculture and Forestry, University of Padova, Agripolis, Viale dell'Università 16, 35020 Legnaro, Italy; dario.friso@unipd.it

Abstract: For many years now, manufacturers have been producing supersonic ejectors with a high entrainment ratio for the chemical, oil, and food industries. In the present work, mathematical modelling of the entrainment ratio of such industrial ejectors is carried out, in which a variation of the diffuser efficiency is also assumed to be a function of the Mach number of the motive gas. To determine this unknown relationship, the mathematical modelling was overturned by inserting the entrainment ratios of ten different high-performance industrial ejectors, as identified through an experimental investigation. The mathematical modelling, completed through the use of the relationship between the diffuser efficiency and the Mach number of the motive gas, was applied to sixty-eight ejectors, built and tested experimentally over the last twenty years as part of research aimed at the development of thermal ejector refrigeration systems (ERSs), to obtain the entrainment ratios proposed by the manufacturers (industrial entrainment ratios). A comparison of the experimental entrainment ratios with respect to the industrial ones demonstrated that the former were always lower, ranging from a minimum of −17% to a maximum of −82%. These results indicate that the lab-built ejectors for ERS prototypes can be improved. Therefore, in the future, researchers should apply numerical analysis iteratively, starting from a given geometry of the ejector, and modifying it until the numerical analysis provides the industrial value of the entrainment ratio.

Keywords: ejector; supersonic; thermo-compressor; entrainment ratio; high performance

Citation: Friso, D. Mathematical Modelling of the Entrainment Ratio of High Performance Supersonic Industrial Ejectors. *Processes* **2022**, *10*, 88. https://doi.org/10.3390/pr10010088

Academic Editor: Md. Shakhaoath Khan

Received: 14 November 2021
Accepted: 29 December 2021
Published: 2 January 2022

1. Introduction

An ejector, or jet pump, is an apparatus (Figure 1) of which the task is the compression of a fluid—called the induced fluid—by molecular entrainment and diffusion, through a jet produced by the expansion of another fluid—called the motive fluid [1,2]. Fluids can be liquid or gas and, in this case, are in supersonic motion. In this work, supersonic ejectors are discussed, as they are widespread in the chemical, oil, and food industries, where they are used in the following:

- Vacuum pumps to eliminate incondensable gases (sucked fluid) in various treatment plants, where the motive fluid is steam from a boiler; or
- Steam compressors in concentration and distillation plants. The vapor resulting from boiling liquid is thermodynamically requalified and then reused to heat the boiling liquid itself. This ejector–heat exchanger system is, therefore, a heat pump, and the ejector is also called a thermo-compressor. Furthermore, in this case, the motive fluid is steam from a boiler.

Various studies focused on the use of supersonic ejectors as thermo-compressors in heat-driven ejector refrigeration systems (ERSs), where both fluids are refrigerating gases, have been underway for many years. This type of system, which has been known for more than a century [3], is now being re-proposed for environmental reasons, as they can operate on solar energy [4].

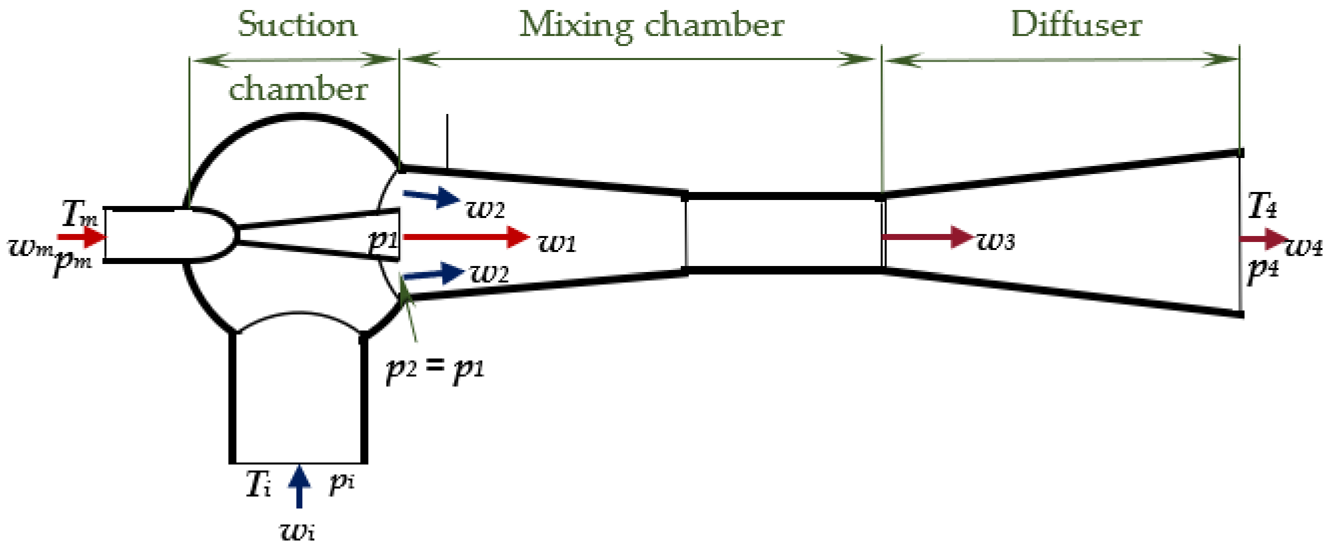

Figure 1. General schematic of an ejector: The motive gas enters on the left with mass flow rate G_m; the induced gas enters from below with mass flow rate G_i.

The peculiarities of these ejectors are as follows: The absence of moving parts and, therefore, reliability and durability; simplicity of construction and, therefore, relatively low investment cost; operational rigidity, as they operate correctly only in design conditions; and the complexity of the phenomena of mixing and diffusion of the two fluids operating in transonic and supersonic conditions, therefore leading to difficulty in the mathematical modelling and design of high-performance ejectors. In confirmation of this last point, it should be noted that there are no more than a dozen manufacturers in the world capable of producing high-performance supersonic ejectors.

The performance of an ejector can be identified by the entrainment ratio ω, defined as the ratio between the mass flow rate of the induced gas G_i to that of the motive gas G_m. Its calculation—and, therefore, prediction of the performance of an ejector—can be carried out with the aid of a one-dimensional gas-dynamics theory. Keenan and Neumann [5] used such a one-dimensional approach with the hypothesis of ideal gas behavior considering the equations of conservation of mass, momentum, and energy; however, they excluded frictional losses and diffusion modelling. In a subsequent work, Keenan, Neumann, and Lustwerk [6] introduced these two phenomena; however, the mathematical description of the dissipative phenomenon of shock waves occurring in the transition from supersonic to subsonic motion of the gas mixture was lacking.

A later work by Lukasiewicz [7] on diffuser ducts highlighted the presence of several curved or oblique shock waves. Furthermore, Shapiro [8], in his 1953 textbook, referred to a series of bifurcated normal shocks in diffuser ducts. Matsuo [2] has called this phenomenon a shock train, but other expressions are also in use, besides those mentioned by Shapiro and Lukasiewicz: a series of shocks [9], Lambda foot shock system [10], Bifurcated normal shock waves [11], a series of oblique shocks [12], multiple normal shocks [13], and multiple shocks [14].

Munday and Bagster [15] introduced a mathematical formulation of the phenomenon of diffusion in the ejector from supersonic to subsonic stream using the Prandtl–Meyer equation, which predicts the presence of a frontal shock wave. Furthermore, they proposed that the induced gas, in the first part of the mixing chamber (Figure 1), remained separate from the motive one and was forced to expand up to the sonic conditions. This was due to widening of the motive gas jet, leading to a reduction in the section available for the induced gas. From the sonic condition of the induced gas, the real mixing hypothesized at constant pressure then started.

With the renewed interest in ejectors used as thermo-compressors in refrigeration cycles, Eames et al. [16] verified this one-dimensional analytical approach for various ejectors inserted in a heat-driven ejector refrigeration system (ERS) operated with steam, noting that the experimental entrainment ratio was always less than that predicted theoretically. Similar differences have also been identified by Huang et al. [17], considering different ejectors inserted in an ERS with refrigerant fluid R141b. Rogdakis and Alexis [18] also experimentally verified the theory with an ejector operating in an ERS with refrigerant fluid R717, always identifying a more optimistic theoretical entrainment ratio.

Therefore, in order of a better comprehension of the phenomena of mixing and diffusion, the computer fluid dynamics CFD modelling is useful. Consequently, for about 20 years, computational studies on the operation and design of ejectors have continued to be produced, focused on both on-design and off-design conditions [19–46]. Most of the results of the numerical analyses presented in these works have been experimentally validated by the authors: in many cases, the entrainment ratio in the on-design condition predicted by the numerical analysis has presented a negligible difference, compared with the experimental one.

Parallel to this incessant scientific commitment—which began over 80 years ago and has accelerated in the last twenty years due to the availability of numerical analysis software—manufacturers of supersonic ejectors for various industrial sectors (i.e., chemical, oil, and food) have been present on the market for over a century.

For example, in Germany, Koerting Gebrueder began manufacturing supersonic ejectors in 1920 and, in 1964, began using computers for the fluid dynamic design of supersonic jet pumps (as ejectors are also called). Therefore, it is very likely that the design guidelines adopted by Koerting AG were not and (even more so today) are not purely empirical. Moreover, in Germany, another company was founded in the 1940s, Wiegand (which has recently been absorbed by GEA AG), by the researcher Joachim Wiegand, who in 1940, published a 24-page booklet full of theory and experimental data on the design of ejectors [47]. In Europe, other relevant manufacturers, such as the French SCAM, Kinetic-therm, and LVI and the Spanish Equirepsa, subsequently established themselves, while in the United States [1], Croll-Reynolds, Fox-Valve, Graham Manufacturing, Jet-vac technologies, and Nash-kinema have long been known. It is likely that some names have been unintentionally forgotten, but it should be noted that there are only a dozen manufacturers internationally, and not all of them produce high-performance ejectors (i.e., with high entrainment ratio = industrial entrainment ratio).

In the first part of this work, we detail an experimental investigation carried out to determine the entrainment ratio values obtainable from high-performance supersonic ejectors designed under different boundary conditions (i.e., pressure and temperature of the motive gas, the induced gas, and the mixed gases at the outlet). These ejectors offer high-performance (optimal entrainment ratio) because they are built by a big European manufacturer that has been present on the international market for 80 years. In the second part, mathematical modelling is carried out, which, starting from the Wiegand equations [47], correlates the entrainment ratio of the aforementioned ejectors of the European manufacturer to the gas properties, the boundary conditions (pressures and temperatures), and the isentropic efficiency of the supersonic nozzle (motive gas), suction chamber (induced gas), and diffuser (mixed gases). In the third part of the work, the mathematical model is used to obtain the values of the entrainment ratio as a function of the gas properties and the boundary conditions (pressures and temperatures) of ejectors built and tested in the laboratory. These ejectors are considered benchmarks, as they are used to test the results of the numerical analyses proposed in many papers.

A comparison between the industrial entrainment ratios predicted from the mathematical model elaborated in the second part and the entrainment ratios obtained experimentally from the benchmark ejectors highlights important differences; namely, the experimental values are always lower than the industrial ones.

This is due to the fact that all of the numerical analyses conducted on the ejectors are characterized by computational thermo-fluid dynamics investigations, which provide entrainment ratio values for given geometries of the elements of the ejector, and all the validations made in the laboratory were used to experimentally check the entrainment ratio predicted by the numerical analysis, but not to improve the geometry in order to maximize the entrainment ratio. This is because numerical analysis does not allow for derivation of the geometry by imposing the value of the entrainment ratio; that is, it does not allow for a direct design [48]. In other words, numerical analyses can estimate, with great precision, the entrainment ratio for a given ejector component geometry without having to build it; however, if one wishes to obtain a high-performance ejector, it is necessary to analyze various geometries, until one having a suitably high entrainment ratio is obtained. On the other hand, maximizing the entrainment ratio involves maximizing the coefficient of performance COP [19] of the ejector refrigeration system ERS. Therefore, it is necessary to know the maximum values of the entrainment ratio that international manufacturers—including that of the ejectors investigated in this work—can obtain and which is the result of thousands of industrial tests and millions of ejectors that have been built and sold.

2. Materials and Methods

2.1. High Performance of Industrial Ejectors

At an Italian company for the construction of food evaporators equipped with ejectors/thermo-compressors purchased from a European company that has manufactured ejectors for 80 years, a survey was conducted to determine the performance, represented by the entrainment ratio, of various industrial ejectors installed in the evaporators. Eight ejectors were identified with a wide variability of boundary conditions—that is, in terms of the pressure of the motive gas p_m, pressure of the induced gas p_i, and pressure of the mixed gases p_4 at the outlet (Figure 1)—to constitute a heterogeneous population.

In Table 1, the operating data of these eight industrial ejectors (ejectors No. 1–8) are presented, including the pressures and stagnation temperatures of the motive gas (p_m and T_m, respectively), those of the induced gas (p_i and T_i, respectively), the outlet pressure (p_4), the mass flow rates of the motive gas (G_m) and the induced gas (G_i), and the diameters of the intake pipes (D_i) and outlet (D_4). All of the ejectors had motive gas consisting of dry saturated steam and induced gas also consisting of dry saturated steam. Finally, Table 1 shows the industrial entrainment ratios ω_{ind} declared by the European manufacturer. They are to be considered optimal, as these ejectors have been improved to have the maximum value of the entrainment ratio ω. The European manufacturer has also declared that their ejectors are sized for a critical pressure p_c that is 5% higher than the outlet pressure p_4 (Figure 2). This is a safety margin to avoid the risk of operating in off-design mode, in which the entrainment ratio ω would drop drastically, stopping the operation of the evaporator in which the ejector is installed.

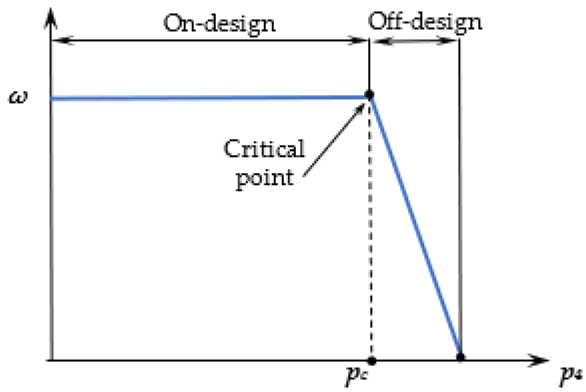

Figure 2. Ejector operating curve: The pressure at the outlet of the diffuser is p_4. To operate correctly—that is, keeping the entrainment ratio constant and equal to the design value (on-design)—the pressure p_4 must be equal to or lower than the critical pressure p_c.

The survey was conducted with an inspection of the evaporators installed in Italy. This survey allowed for verification of the regular operation of the evaporators and, therefore, of the installed ejectors. It could not be otherwise, as this European manufacturer is a company that is known internationally and has operated for eighty years in the construction of ejectors.

Table 1. Operating data of the high-performance industrial ejectors.

Ejector N.	**1**	**2**	**3**	**4**	**5**	**6**	**7**	**8**	**9**	**10**
Motive gas	Steam	Steam	Steam	Steam	Steam	Steam	Steam	Steam	Steam	Steam
Motive gas pressure p_m (bar)	6	9	9	9	10	12	10	8	5	5
Motive gas temperature t_m (°C)	159	175	175	175	180	188	180	170	152	152
Induced gas	Steam	Steam	Steam	Steam	Steam	Steam	Steam	Steam	Air	Air
Induced gas pressure p_i (bar)	0.520	0.380	0.0958	0.0316	0.0424	0.533	0.0131	0.123	0.5	0.3
Ind. gas temperature t_i (°C)	82	75	45	25	30	83	11	50	20	20
Aspiration diameter D_i (mm)	125	200	300	500	350	125	200	250	50	50
Discharge pressure p_4 (bar)	1.013	0.8	0.265	0.0732	0.096	1.720	0.096	0.31	1.013	1.013
Discharge diameter D_4 (mm)	150	200	300	500	350	150	200	250	50	50
Critical pressure $p_c = 1.05 \cdot p_4$ (bar)	1.053	0.842	0.279	0.0771	0.101	1.811	0.101	0.326	1.053	1.053
Motive mass flow rate G_m (kg h^{-1})	1160	1270	1575	1100	550	1900	235	842	128	128
Induced mass flow rate G_i (kg h^{-1})	850	1130	1295	1341	700	680	95	750	104	49
Industrial entrainment ratio ω_{ind}	0.735	0.890	0.822	1.220	1.270	0.358	0.404	0.890	0.810	0.380

In addition, ejectors No. 9 and 10 are two ejectors from the same European company, subjected to tests at the Food Processes Engineering Laboratory at the TESAF Dept. of University of Padova. The two ejectors had motive gas consisting of dry saturated steam produced by a boiler operating at p_m = 5 bar and G_m = 128 kg h^{-1} (Figure 3a), and the induced gas consisting of air at pressure of 0.3 and 0.5 bar, respectively, due to the use of a multiple-orifice device (flute) built according to the guidelines of Power [1]. The tests (Figure 3b) confirmed the performances—represented by the entrainment ratio ω_{ind}—declared by the manufacturer, as shown in Table 1.

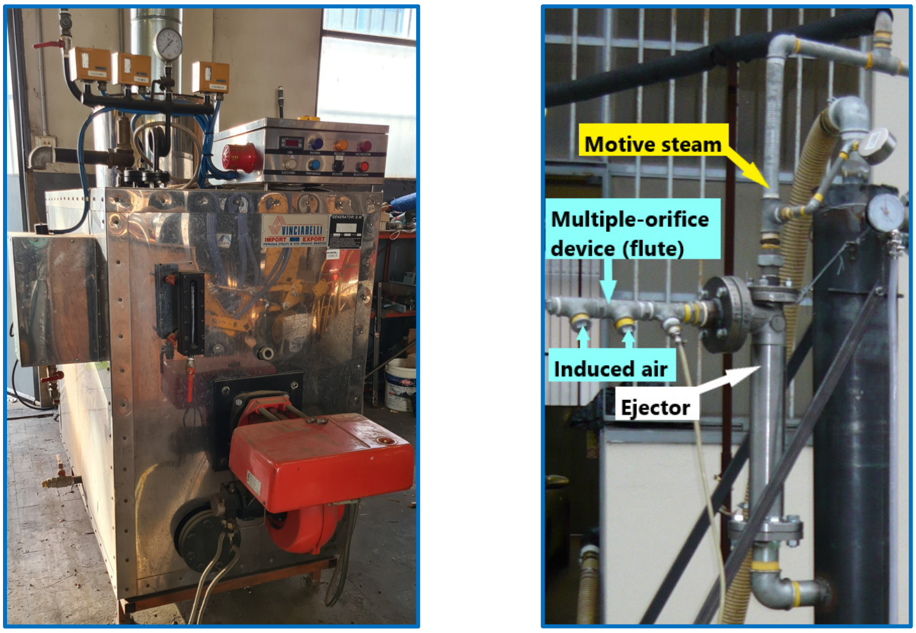

(**a**) (**b**)

Figure 3. Bench tests of the ejectors 9 and 10: (**a**) Motive steam generator; (**b**) Ejectors during the tests: the induced gas was air, which passes through the calibrated orifices of the flute at sonic speed. The number and diameter of the orifices must be calibrated appropriately, in order to produce the suction mass flow rate G_i and the pressure p_i at the inlet of the suction chamber.

2.2. Mathematical Modelling

2.2.1. Calculation of the Pressure at the Outlet of the Suction Chamber and the Diffuser Efficiency of High-Performance Industrial Ejectors

Below, a mathematical model is developed to determine the entrainment ratio, with respect to the pressure and temperature of the motive gas (p_m and T_m, respectively), the pressure and temperature of the induced gas (p_i and T_i, respectively), the pressure of the mixed gases at the outlet (p_4), the physical properties of the gases themselves, and the isentropic efficiencies, which take into account the frictional effects during expansion and diffusion.

Figure 1 presents the schematic of an ejector, in which an appropriate acceleration of the fluid induced in the suction chamber is provided to reduce the speed difference between the two gases in the mixing chamber [49], therefore reducing irreversibility. In this way, an increase in the entrainment ratio is achieved.

The momentum theorem applied to the mixing chamber [47,50,51], neglecting pressure variations and friction with the mixing chamber wall, gives the following:

$$w_1 \cdot G_m + w_2 \cdot G_i = w_3 \cdot (G_m + G_i), \tag{1}$$

where G_m is the mass flow rate of the motive gas (kg s^{-1}), w_1 is the supersonic velocity of the motive stream at the inlet of the mixing chamber (m s^{-1}), G_i is the mass flow rate of the induced gas (kg s^{-1}), and w_2 is the subsonic velocity of the induced stream at the inlet of the mixing chamber (m s^{-1}). It should be noted that, unlike Eames [3] and other subsequent researchers, the mixing efficiency η_m is not included in Equation (1); that is, following the old German school, η_m is considered unitary.

By defining the entrainment ratio as $\omega = G_i/G_m$, from Equation (1), we obtain the following:

$$\omega = \frac{w_1 - w_3}{w_3 - w_2}. \tag{2}$$

The three speeds inside the ejector (w_1, w_2, and w_3) can be obtained from the energy equation (first law of thermodynamics) [8,50] applied to the irreversible adiabatic steady flow, as follows:

1. Motive stream in the nozzle:

$$w_1 = \sqrt{2 \cdot \eta_{E1} \cdot \Delta h_1}, \tag{3}$$

2. Induced stream in the suction chamber:

$$w_2 = \sqrt{2 \cdot \eta_{E2} \cdot \Delta h_2}, \tag{4}$$

3. Mixed stream in the mixing chamber:

$$w_3 = \sqrt{2 \cdot \frac{\Delta h_3}{\eta_D}}, \tag{5}$$

where Δh_1, Δh_2, and Δh_3, are the isentropic difference in enthalpies of the motive stream in the nozzle, induced stream in the suction chamber, and mixed stream in the diffuser, respectively; η_{E1} is the isentropic efficiency in the nozzle; η_{E2} is the isentropic efficiency in the suction chamber; and η_D is the isentropic efficiency of the diffuser, which accounts for the whole loss during the pressure gain process due to the shock train and subsonic diffuser section.

In Equations (3)–(5), the velocities of the gases in the m, i, and 4 sections of the ejector (i.e., w_m, w_i, and w_4; see Figure 1) have been omitted, as the corresponding kinetic energies are smaller than 2% of those corresponding to the velocities inside the ejector (i.e., w_1, w_2, and w_3).

By introducing Equations (3)–(5) into Equation (2), we obtain the following:

$$\omega = \frac{\sqrt{\eta_{E1} \cdot \eta_D \cdot \Delta h_1} - \sqrt{\Delta h_3}}{\sqrt{\Delta h_3} - \sqrt{\eta_{E2} \cdot \eta_D \cdot \Delta h_2}}. \quad (6)$$

The isentropic difference in enthalpies for the ideal gas—a valid model for the gases operating in the ejector—are as follows:

4. Motive stream in the nozzle:

$$\Delta h_1 = \frac{k_m}{k_m - 1} R_m \cdot T_m \left[1 - \left(\frac{p_1}{p_m} \right)^{\frac{k_m - 1}{k_m}} \right], \quad (7)$$

5. Induced stream in the suction chamber:

$$\Delta h_2 = \frac{k_i}{k_i - 1} R_i \cdot T_i \left[1 - \left(\frac{p_2}{p_i} \right)^{\frac{k_i - 1}{k_i}} \right], \quad (8)$$

6. Mixed stream in the diffuser:

$$\Delta h_3 = \frac{k_4}{k_4 - 1} R_4 \cdot T_4 \left[1 - \left(\frac{p_3}{p_4} \right)^{\frac{k_4 - 1}{k_4}} \right], \quad (9)$$

where k_m is the ratio of specific heats c_p/c_v of the motive gas; k_i is the ratio of specific heats c_p/c_v of the induced gas; k_4 is the ratio of specific heats c_p/c_v of the mixed gases; R_m is the specific constant of the motive gas; R_i is the specific constant of the induced gas; R_4 is the specific constant of the mixed gases; p_1 is the pressure of the motive gas at the exit of the nozzle, which is equal to p_2; p_2 is the pressure of the induced gas at the exit of the suction chamber, which is equal to the pressure at the inlet of mixing chamber; p_m is the pressure of the motive gas at the inlet of the nozzle; p_i is the pressure of the induced gas at the inlet of the suction chamber; p_3 is the pressure of the mixed gas at the end of mixing chamber, which is supposed to be equal to the pressure at the inlet of mixing chamber p_2 (isobaric process of mixing); p_4 is the pressure of the mixed gases at the exit of the diffuser; and T_m is the absolute stagnation temperature (K) of the motive gas, which is supposed to be equal to the absolute temperature at the inlet of nozzle (t_m is the same temperature in °C); T_i is the absolute stagnation temperature of the induced gas, which is supposed to be equal to the absolute temperature at the inlet of the suction chamber; and T_4 is the absolute stagnation temperature of the mixed gases, which is supposed to be equal to the absolute temperature at the exit of the diffuser.

The equations for the calculation of the specific heat at constant pressure c_{p4} and that at constant volume c_{v4}, the ratio of specific heats k_4, the absolute stagnation temperature T_4, and the specific constant of the mixed gases R_4 are provided in Appendix A.

By combining Equations (6)–(9), we obtain the following:

$$\omega = \frac{\sqrt{\eta_{E1} \cdot \eta_D \cdot \frac{k_m}{k_m - 1} R_m \cdot T_m \left[1 - \left(\frac{p_2}{pm} \right)^{\frac{k_m - 1}{k_m}} \right]} - \sqrt{\frac{k_4}{k_4 - 1} R_4 \cdot T_4 \left[1 - \left(\frac{p_2}{p4} \right)^{\frac{k_4 - 1}{k_4}} \right]}}{\sqrt{\frac{k_4}{k_4 - 1} R_4 \cdot T_4 \left[1 - \left(\frac{p_2}{p4} \right)^{\frac{k_4 - 1}{k_4}} \right]} - \sqrt{\eta_{E2} \cdot \eta_D \cdot \frac{k_i}{k_i - 1} R_i \cdot T_i \left[1 - \left(\frac{p_2}{pi} \right)^{\frac{k_i - 1}{k_i}} \right]}} \quad (10)$$

In this equation, considering the appropriate design of the nozzle, the high Reynolds number, and the accelerating flow with the consequence of a very thin boundary layer compared to the nozzle section, the isentropic efficiency of the nozzle η_{E1} has limited variation, ranging from 0.95 to 0.99 [8,19]. Furthermore, the isentropic efficiency of the suction chamber η_{E2}, before the mixing chamber, also has limited variation (from 0.92 to 0.99) [8,19]. For caution, here, η_{E1} is assumed to have a constant value of 0.95 and η_{E2} has a constant value of 0.92, as the wall of the suction chamber is considered to be rough.

In the diffusion process from the last part of the mixing chamber to the ejector outlet, the isentropic efficiency η_D is not constant, due the presence of a shock train. In a similar case considering a cylindrical diffuser with initial supersonic motion, Shapiro [8] indicated that η_D is dependent of the inlet Mach number. In this work, a dependence of η_D on the Mach number of the motive stream at the nozzle exit, M_{m-2}, was found; this Mach number is as follows [52]:

$$M_{m-2} = \sqrt{\frac{2 \cdot \eta_{E1}}{k_m - 1}\left[\left(\frac{p_m}{p_2}\right)^{\frac{k_m-1}{k_m}} - 1\right]}. \tag{11}$$

Equation (10) shows that the entrainment ratio, ω, depends on two important variables: the efficiency of the diffuser η_D and the pressure of induced gas at the exit of suction chamber p_2, which is equal to the pressure at the nozzle exit p_1 (Figure 1).

The diagram shown in Figure 4 represents the function of the entrainment ratio ω with respect to the pressure p_2 and the isentropic efficiency of the diffuser η_D; that is, $\omega = f(p_2, \eta_D)$.

The diagram shows that, for each diffusion efficiency value η_D, the function $\omega = f(p_2)$ has a maximum (Figure 5). Therefore, the entrainment ratio ω has a maximum value corresponding to a precise value of the pressure p_2, which accelerates the induced gas such that the lower speed difference between the motive gas and the induced gas reduces the frictional effects in the mixing chamber, while avoiding an excessive compression ratio in the diffuser which, instead, negatively affects the entrainment ratio.

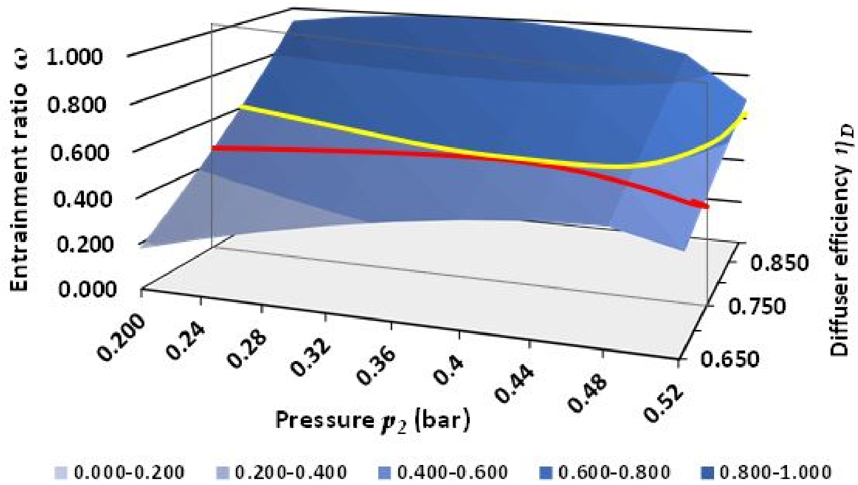

Figure 4. Diagram (derived from Equation (10)) of the entrainment ratio of an ejector (N. 1, Table 1) vs. pressure at the exit of the suction chamber p_2 and the diffuser efficiency η_D: $\omega = f(p_2, \eta_D)$. The red curve represents the function: $\omega = f(p_2)$. The yellow curve represents the function: $\eta_D = f(p_2)$. The p_2 pressure value that maximizes the entrainment ratio ω is also the one that minimizes the diffuser efficiency η_D.

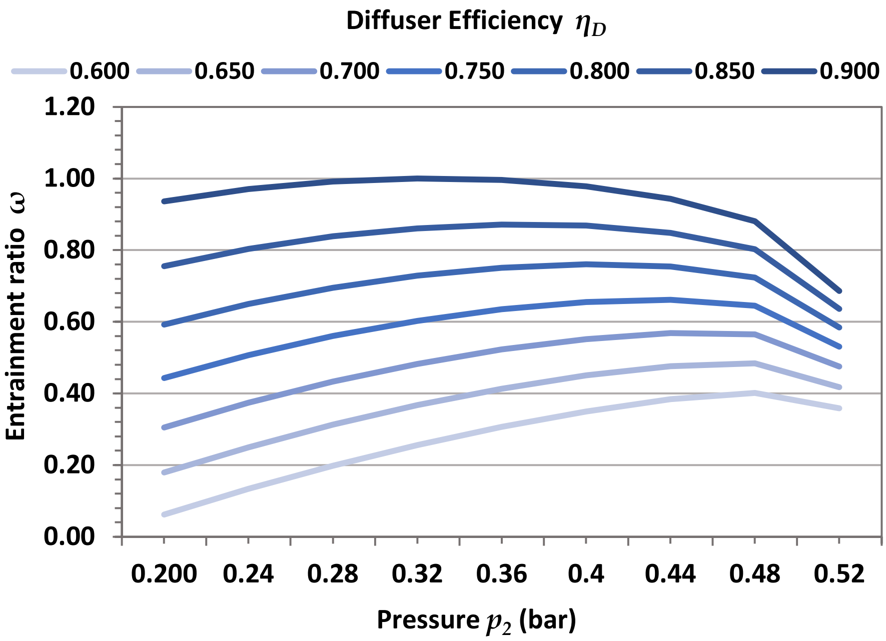

Figure 5. Function: $\omega = f(p_2)$ parametric in η_D.

The values of the entrainment ratio ω_{ind} presented in Table 1 concern high-performance industrial ejectors, in which the manufacturer has also foreseen the correct acceleration of the induced stream in the suction chamber to obtain the high entrainment ratio (i.e., ω_{ind}). If these ω_{ind} values are introduced into (10), the equation is left with two unknowns: The pressure p_2 and the diffuser efficiency η_D. It seems to be a problem without solution, but studying the function $\omega = f(p_2)$, which is parametric in η_D (shown in Figure 5), as well as the function $\eta_D = f(p_2)$, which is parametric in ω (shown in Figure 6) we find that when the former, $\omega = f(p_2)$, presents its maximum, the latter, $\eta_D = f(p_2)$, presents its minimum.

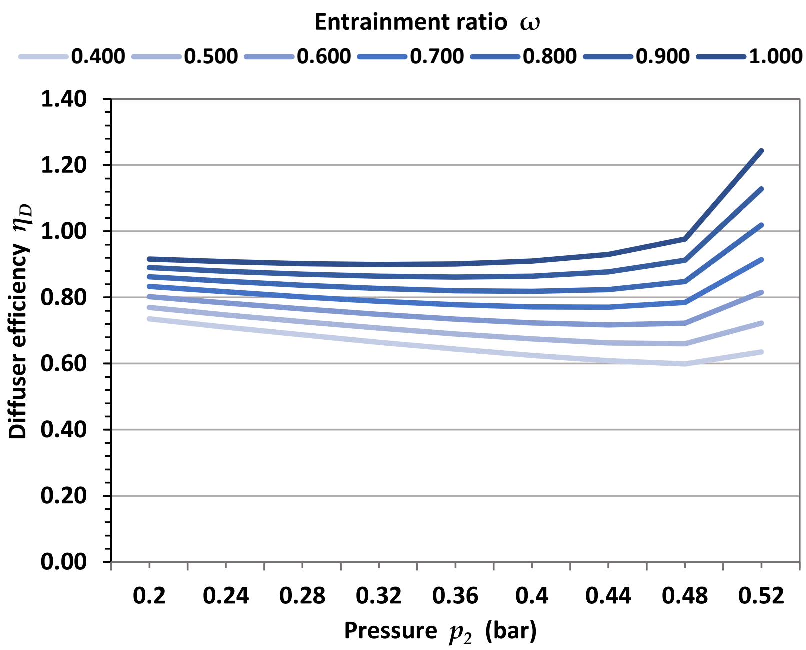

Figure 6. Function: $\eta_D = f(p_2)$ parametric in ω.

Therefore, it is possible to determine the value of p_2 that minimizes the isentropic efficiency of the diffuser, by zeroing the derivative of the function $\eta_D = f(p_2, \omega)$, providing the parameter ω with the values ω_{ind} in Table 1 for the high-performance industrial ejectors. The solution provides p_2 values that minimize the diffuser efficiency while also maximizing the entrainment ratio. The function $\eta_D = f(p_2, \omega_{ind})$ is obtained from (10):

$$\eta_D = \frac{\frac{k_4}{k_4-1} R_4 \cdot T_4 \left[1 - \left(\frac{p_2}{p_4}\right)^{\frac{k_4-1}{k_4}}\right] \cdot (1 + \omega_{ind})^2}{\left\{\sqrt{\eta_{E1} \cdot \frac{k_m}{k_m-1} R_m \cdot T_m \left[1 - \left(\frac{p_2}{p_m}\right)^{\frac{k_m-1}{k_m}}\right]} + \sqrt{\omega_{ind}^2 \cdot \eta_{E2} \cdot \frac{k_i}{k_i-1} R_i \cdot T_i \left[1 - \left(\frac{p_2}{p_i}\right)^{\frac{k_i-1}{k_i}}\right]}\right\}^2} \tag{12}$$

Taking the derivative of (12) and equating it to zero, we have the following:

$$\frac{\partial \eta_D}{\partial p_2} = \frac{-R_4 \cdot T_4 \cdot \frac{(p_2)^{-\frac{1}{k_4}}}{(p_4)^{\frac{k_4-1}{k_4}}} \cdot (1+\omega_{ind})^2}{\left[\sqrt{F_m} + \sqrt{\omega_{ind}^2 \cdot F_i}\right]^2} + \frac{2 \cdot F_4 \cdot (1+\omega_{ind})^2 \left[\frac{\eta_{E1} \cdot R_m \cdot T_m \cdot \frac{(p_2)^{-\frac{1}{k_m}}}{(p_m)^{\frac{k_m-1}{k_m}}}}{\sqrt{F_m}} + \frac{\omega_{ind}^2 \cdot \eta_{E2} \cdot R_i \cdot T_i \cdot \frac{(p_2)^{-\frac{1}{k_i}}}{(p_i)^{\frac{k_i-1}{k_i}}}}{\sqrt{\omega_{ind}^2 \cdot F_i}}\right]}{\left[\sqrt{F_m} + \sqrt{\omega_{ind}^2 \cdot F_i}\right]^3} = 0, \tag{13}$$

where F_m, F_i, and F_4 are defined as follows:

$$F_m = \eta_{E1} \cdot \frac{k_m}{k_m - 1} R_m \cdot T_m \left[1 - \left(\frac{p_2}{p_m}\right)^{\frac{k_m-1}{k_m}}\right], \tag{14}$$

$$F_i = \eta_{E2} \cdot \frac{k_i}{k_i - 1} R_i \cdot T_i \left[1 - \left(\frac{p_2}{p_i}\right)^{\frac{k_i-1}{k_i}}\right], \tag{15}$$

$$F_4 = \frac{k_4}{k_4 - 1} R_4 \cdot T_4 \left[1 - \left(\frac{p_2}{p_4}\right)^{\frac{k_4-1}{k_4}}\right]. \tag{16}$$

Equation (13), which can be solved an iterative method, provides the value of p_2 that improves the ejector, as it is also the one that maximizes the entrainment ratio ω.

The value of p_2, inserted into Equation (12), allows us to obtain the efficiency of the diffuser η_D in high-performance industrial ejectors.

As mentioned above, it is to be expected that η_D depends on the Mach number of the motive gas in the second section, M_{m-2}, at the inlet of the mixing chamber. As already said, the calculation method of p_2 described by Equation (13) and that of η_D through Equation (12) can be applied to the high-performance industrial ejectors detailed in Table 1. The obtained p_2 values also allow for obtaining the Mach number, M_{m-2}, through Equation (11). Therefore, the relation $\eta_D = f(M_{m-2})$ can be easily found, as discussed in the results section.

2.2.2. Calculation of the Entrainment Ratio for Ejectors to Be Improved

The calculation of the Mach number M_{m-2} of the motive stream passing from the pressure p_m to the best pressure p_2 requires determination of p_2, which is still unknown.

This means that an iterative calculation procedure must be implemented; however, this can be avoided if the Mach number M_{m-2} is replaced by the Mach number M_{m-i} of the motive stream at the final pressure equal to the suction pressure p_i (Figure 1). In fact, p_i is known as it is a boundary condition of the ejector. As detailed in the results, the equation $\eta_D = f(M_{m-2})$ obtained by regression (Figure 7) by the procedure of Section 2.2.1, has a good coefficient of determination R^2, but the function $\eta_D = f(M_{m-i})$ (Figure 8) has a higher R^2. This is a good reason to always use the relationship $\eta_D = f(M_{m-i})$. Therefore, the procedure for calculating the entrainment ratio ω, as outlined below, begins with the calculation of M_{m-i}:

$$M_{m-i} = \sqrt{\frac{2 \cdot \eta_{E1}}{k_m - 1}\left[\left(\frac{p_m}{p_i}\right)^{\frac{k_m-1}{k_m}} - 1\right]}. \tag{17}$$

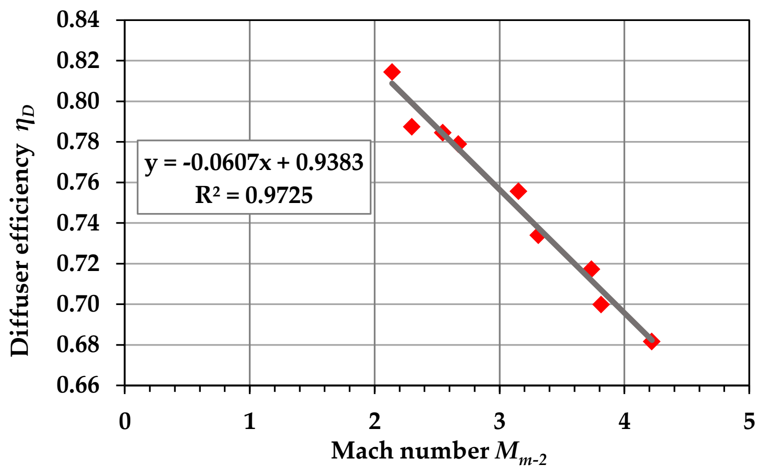

Figure 7. Experimental relationship between the diffuser efficiency η_D and the Mach number M_{m-2} of the motive gas at the final pressure p_2.

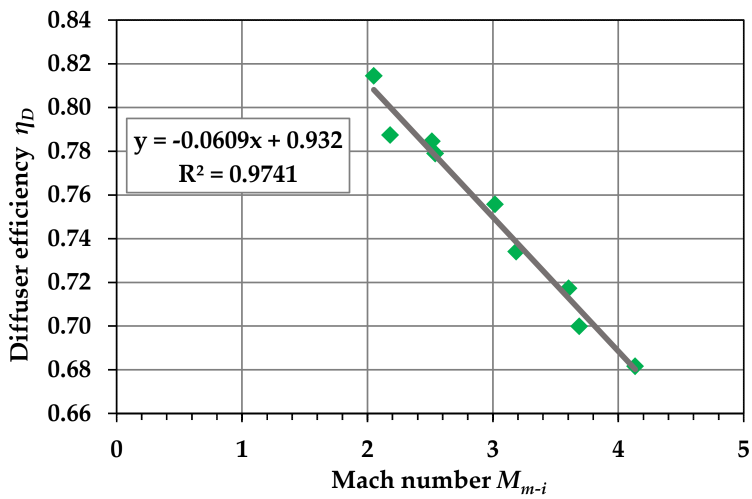

Figure 8. Experimental relationship between the diffuser efficiency η_D and the Mach number M_{m-i} of the motive gas at the final pressure p_i.

The next calculation concerns the efficiency of the diffuser η_D through the function $\eta_D = f(M_{m-i})$, as presented in the results (Section 3.1).

Setting the derivative of Equation (10) equal to zero allows us to obtain the value of the best pressure p_2 which maximizes the entrainment ratio ω:

$$\begin{aligned}\frac{\partial\omega}{\partial p_2} = &\left[\frac{R_4\cdot T_4\cdot \frac{(p_2)^{-\frac{1}{k_4}}}{(p_4)^{\frac{k_4-1}{k_4}}}}{\sqrt[2]{F_4}} - \frac{\eta_D\cdot\eta_{E1}\cdot R_m\cdot T_m\cdot \frac{(p_2)^{-\frac{1}{k_m}}}{(p_m)^{\frac{k_m-1}{k_m}}}}{\sqrt[2]{\eta_D F_m}}\right]\left(\sqrt{F_4}-\sqrt{\eta_D F_i}\right)^{-1} \\ &-\left\{\left[\frac{\sqrt{\eta_D F_m}-\sqrt{F_4}}{\sqrt[2]{\eta_D F_i}}\right]\left(\eta_D\cdot\eta_{E2}\cdot R_i\cdot T_i\cdot\frac{(p_2)^{-\frac{1}{k_i}}}{(p_i)^{\frac{k_i-1}{k_i}}}\right)\right. \\ &\left.-\left[\frac{R_4\cdot T_4\cdot \frac{(p_2)^{-\frac{1}{k_4}}}{(p_4)^{\frac{k_4-1}{k_4}}}}{\sqrt[2]{F_4}}\right]\right\}\left(\sqrt{F_4-\eta_D F_i}\right)^{-2} = 0,\end{aligned} \tag{18}$$

where F_m, F_i, and F_4 are given by Equations (14)–(16), respectively.

Equation (18), similar to Equation (13), also requires solution through an iterative method, for example, by a spreadsheet.

Finally, the pressure value p_2 obtained from Equation (18) allows for obtaining the entrainment ratio ω_{ind} maximized through Equation (10).

The solution of Equations (18) and (10) requires knowledge of the values of k_4, R_4, and T_4 which, according to Equations (A1)–(A5), presented in Appendix A, depend on the unknown value of the entrainment ratio ω.

If the induced gas is equal to the motive gas, then $k_m = k_i = k_4$ and $R_m = R_i = R_4$, but the need remains to determine the stagnation temperature T_4 through Equation (A5), starting from the stagnation temperatures T_m and T_i and from the entrainment ratio ω. The absolute stagnation temperatures T_4, T_m, and T_i practically coincide with the absolute temperatures as (see Figure 1), in Section 4, m, and i, the gases generally have velocities lower than 50 m s^{-1}, often around 30 m s^{-1}. The problem arises of needing to know ω a priori to calculate T_4 which, in turn, serves to calculate the same ω by Equation (18). The problem can be overcome by inserting into the spreadsheet, before Equations (18) and (10), a cell containing an initial value of ω (experience suggests ω = 1) and cells containing Equations (A1)–(A5), which provide the values of c_{p4}, c_{v4}, R_4, k_4, and T_4 resulting from this initial ω. Additionally, it is necessary to enter an initial value for p_2 (experience suggests $p_2 = 0.99\cdot p_i$).

Therefore, the procedure includes the following:

(1) Execution of the iterative method (e.g., by spreadsheet) to search for the ω value associated to $p_2 = 0.99\cdot p_i$, using Equation (10);
(2) Execution of the iterative method (e.g., by spreadsheet) to search for the best value of p_2, using Equation (18);
(3) Final execution of the iterative method (e.g., by spreadsheet) to recalculate the final industrial ω value, now for the best p_2 obtained in step 2, by Equation (10); and
(4) Final execution of the iterative method (e.g., by spreadsheet) to recalculate the final best p_2 value, using Equation (18).

Only two iterations of steps (1) and (3) are sufficient to maximize ω and only two for steps (2) and (4) are required to improve p_2, as the solution method is strongly convergent.

2.3. Experimental Entrainment Ratio of Benchmark Ejectors Built and Tested to Use in ERSs

Benchmark ejectors built and tested by various researchers in their laboratories over the past twenty years, for use in ERS prototypes, have been considered. Details on an initial series of such benchmark ejectors, in terms of their geometric characteristics, boundary conditions, and performance (represented by the entrainment ratio measured in the laboratory) have been presented in the work of Besagni [19] exactly in its Tables 6, 7 and 11.

To check whether these ejectors were improved (i.e., if they were high-performance ejectors), the mathematical model for calculating the industrial high entrainment ratio ω_{ind} proposed in this work was applied.

For some of these ejectors, only the experimental values of the boundary conditions and the entrainment ratio corresponding to the critical point were available while, for others, these values were available both in on-design and off-design contexts (Figure 2). For the latter, using the results reported by [19], the value of the entrainment ratio ω and the corresponding outlet pressure p_4 of the critical point were identified. The critical point was not always uniquely identifiable. Therefore, in these cases, two pairs of ω–p_4 values were taken into consideration, that is, those that could be closest (one to the right and one to the left) to the ω–p_4 pair of the critical point.

Therefore, Table 2 summarizes the values of the boundary conditions and the experimental entrainment ratio ω_{exp} corresponding to the critical point for each ejector, except in some cases, in which there were two critical pseudo-points, marked with the symbol *. The alphanumeric codes reported, which distinguish each ejector (e.g., A1f), are the same as those used in [19].

Table 2. Operating data of the first series of benchmark ejectors built and tested experimentally by the authors indicated in the first column.

Ref.	Geom. [19]	Case [19]	Run [19]	Motive Gas	Induced Gas	p_m (bar)	T_m (°C)	p_i (bar)	T_i (°C)	$p_4 = p_c$ (bar)	ω_{exp}
[53]	A	1	f	Steam	Steam	3.6	139.8	0.032	25	0.053	1.2
[54]	M	1	i	Steam	Steam	2.703	130	0.012	10	0.05	0.4
[54]	M	2	e	Steam	Steam	1.987	120	0.012	10	0.038	0.513
[54]	M	3	g	Steam	Steam	2.703	130	0.009	5	0.048	0.31
[55]	B	1	d	R1234ze	R1234ze	11.79	63.7	2.18	8.4	5.09	0.24
[55]	B	2	c	R1234ze	R1234ze	11.60	64.7	2.72	11	4.92	0.408
[56]	C	1	h*	R134a	R134a	26.33	100	3.5	15	7.2	0.329
[56]	C	1	p*	R134a	R134a	26.33	100	3.5	15	8.0	0.252
[56]	C	2	d*	R134a	R134a	26.33	100	3.82	17.6	7.5	0.393
[56]	C	2	k*	R134a	R134a	26.33	100	3.82	17.6	8.2	0.293
[56]	C	3	d*	R134a	R134a	26.33	100	4.25	20.7	7.7	0.489
[56]	C	3	h*	R134a	R134a	26.33	100	4.25	20.7	8.3	0.390
[56]	C	4	e*	R134a	R134a	26.33	100	4.65	23.5	7.8	0.554
[56]	C	4	i*	R134a	R134a	26.33	100	4.65	23.5	8.5	0.438
[57]	F	1		R134a	R134a	23.33	84.2	4.15	20	6.5	0.592
[57]	F	2		R134a	R134a	31.90	100	3.50	15	6.9	0.361
[57]	F	3		R134a	R134a	31.90	100	4.15	20	6.9	0.433
[58]	I	1	c*	R134a	R134a	28.89	94.4	4.146	20	7.32	0.459
[58]	I	1	d*	R134a	R134a	28.89	94.4	4.146	20	7.54	0.416
[58]	J	1	d	R134a	R134a	28.89	94.4	4.146	20	7.5	0.476
[58]	K	1	e	R134a	R134a	28.89	94.4	4.146	20	7.66	0.504
[59]	G	1	c	R245fa	R245fa	11.298	95	0.758	8	1.979	0.31
[59]	G	2	c	R245fa	R245fa	11.298	95	0.895	12	2.083	0.4
[59]	G	3	b*	R245fa	R245fa	11.298	95	1.052	16	2.120	0.55
[59]	G	3	c*	R245fa	R245fa	11.298	95	1.052	16	2.202	0.48
[59]	H	1	b*	R245fa	R245fa	11.298	95	0.758	8	1.845	0.41
[59]	H	1	c*	R245fa	R245fa	11.298	95	0.758	8	1.901	0.34
[59]	H	2	b*	R245fa	R245fa	11.298	95	0.895	12	1.911	0.54
[59]	H	2	c*	R245fa	R245fa	11.298	95	0.895	12	2.008	0.48
[59]	H	3	b*	R245fa	R245fa	11.298	95	1.052	16	1.979	0.68
[59]	H	3	c*	R245fa	R245fa	11.298	95	1.052	16	2.116	0.59
[60]	D	1	f*	R141b	R141b	6.773	100	0.435	10	1.050	0.247
[60]	D	1	g*	R141b	R141b	6.773	100	0.435	10	1.070	0.239
[60]	D	2	f*	R141b	R141b	6.773	100	0.336	4	1.037	0.123
[60]	D	2	g*	R141b	R141b	6.773	100	0.336	4	1.059	0.116
[60]	D	3	f	R141b	R141b	6.773	100	0.256	−2	1.027	0.063
[61]	L	1	f	Air	Air	10.0	25	5.0	25	6.0	0.452

A second series of benchmark ejectors, with their geometric characteristics, boundary conditions, and performance represented by the entrainment ratio measured in the laboratory, was found in the works [62–66], as summarized in Table 3.

Table 3. Operating data of the second series of benchmark ejectors built and tested experimentally by the authors indicated in the first column.

Ref.	Figure of Ref.	Case	Run	Motive Gas	Induced Gas	p_m (bar)	T_m (°C)	p_i (bar)	T_i (°C)	$p_4 = p_c$ (bar)	ω_{exp}
[62]	4a	CON	13.4-D1.4	Steam	Steam	2.701	130	0.01036	7.5	0.04575	0.367
[62]	4a	CON	19-D2.0	Steam	Steam	2.701	130	0.01036	7.5	0.04575	0.367
[62]	4a	CON	13.4-D1.7	Steam	Steam	2.701	130	0.01036	7.5	0.0580	0.188
[62]	4a	CON	19-D2.4	Steam	Steam	2.701	130	0.01036	7.5	0.0655	0.167
[62]	4b	CON	D1.4	Steam	Steam	2.701	130	0.01036	7.5	0.0456	0.276
[62]	4b	CRMC	D1.4	Steam	Steam	2.701	130	0.01036	7.5	0.0444	0.390
[62]	4b	CON	D1.7	Steam	Steam	2.701	130	0.01036	7.5	0.0582	0.190
[62]	4b	CRMC	D1.7	Steam	Steam	2.701	130	0.01036	7.5	0.0562	0.267
[63]	5	p_m	116	Steam	Steam	1.160	104	0.01306	11	0.0237	0.617
[63]	5	p_m	153	Steam	Steam	1.530	112	0.01306	11	0.0294	0.486
[63]	5	p_m	198	Steam	Steam	1.980	120	0.01306	11	0.0392	0.389
[63]	5	p_m	270	Steam	Steam	2.700	130	0.01306	11	0.0475	0.343
[63]	6	p_i	1.306	Steam	Steam	1.980	120	0.01306	11	0.0392	0.389
[63]	6	p_i	1.933	Steam	Steam	1.980	120	0.01933	17	0.0409	0.643
[63]	6	p_i	2.346	Steam	Steam	1.980	120	0.02346	20	0.0418	0.769
[64]	9	p_m	350	Steam	Steam	3.50	139	0.70	90	1.231	0.430
[64]	9	p_m	450	Steam	Steam	4.50	148	0.70	90	1.517	0.324
[64]	9	p_m	550	Steam	Steam	5.50	155.5	0.70	90	1.804	0.222
[64]	10	p_i	90	Steam	Steam	4.50	148	0.90	96.7	1.560	0.464
[64]	10	p_i	70	Steam	Steam	4.50	148	0.70	90	1.517	0.324
[64]	10	p_i	50	Steam	Steam	4.50	148	0.50	81.3	1.477	0.181
[65]	3	p_i	90	R245fa	R245fa	5.57	84	0.90	12	2.171	0.132
[65]	3	p_i	95	R245fa	R245fa	5.57	84	0.95	14	2.182	0.152
[65]	3	p_i	100	R245fa	R245fa	5.57	84	1.00	15	2.193	0.172
[65]	3	p_i	105	R245fa	R245fa	5.57	84	1.05	16	2.205	0.193
[65]	3	p_i	110	R245fa	R245fa	5.57	84	1.10	17	2.216	0.213
[65]	3	p_i	115	R245fa	R245fa	5.57	84	1.15	18	2.227	0.233
[65]	3	p_i	120	R245fa	R245fa	5.57	84	1.20	19	2.240	0.251
[66]	3	p_m	2148	R134a	R134a	21.480	71	3.1	2	4.680	0.626
[66]	3	p_m	2340	R134a	R134a	23.400	75	3.1	2	5.120	0.528
[66]	3	p_m	2495	R134a	R134a	24.950	77	3.1	2	5.330	0.481

3. Results

3.1. High-Performance Industrial Ejectors

For the ten high-performance industrial ejectors produced by the European manufacturer, Equation (13) was applied, together with Equations (A1)–(A5), in order to determine the best values of the pressure p_2 (Table 4) of the induced gas at the exit of the suction chamber. It should be noted that the value of the specific heat ratio of motive steam, k_m, used in the calculations, was not equal to 1.3 (typical of superheated steam), but was equal to an average empirical value of 1.14 (which corresponds to wet steam) [67]. In fact, the motive steam, during the expansion in the nozzle starting from the dry saturated condition, assumes the wet condition. The k_i value was also equal to 1.14 for the first eight ejectors, which intake dry saturated steam which, when expanded in the suction chamber, became wet steam. Meanwhile, for ejectors 9 and 10, which intake air, k_i was set to 1.4.

Table 4. Results of mathematical modelling applied to high-performance industrial ejectors to calculate diffuser efficiency.

Ejector N.	1	2	3	4	5	6	7	8	9	10
Industrial entrainment ratio ω_{ind}	0.735	0.890	0.822	1.220	1.270	0.358	0.404	0.890	0.810	0.380
Diffuser efficiency η_D	0.788	0.779	0.734	0.700	0.717	0.744	0.682	0.756	0.815	0.785
Pressure of induced gas p_i (bar) at the inlet of suction chamber	0.520	0.380	0.0958	0.0316	0.0424	0.533	0.0131	0.123	0.5	0.3
Pressure of induced gas p_2 (bar) at the exit of suction chamber	0.4136	0.2888	0.0725	0.0239	0.0315	0.4549	0.0109	0.0913	0.4077	0.2562
Mach number M_{i-2} of induced gas at the pressure p_2	0.612	0.672	0.676	0.676	0.699	0.508	0.553	0.700	0.526	0.461
Mach number M_{m-2} of motive gas at the final pressure p_2	2.297	2.671	3.311	3.813	3.737	2.591	4.220	3.152	2.212	2.445
Mach number M_{m-i} of motive gas at the final pressure p_i	2.180	2.539	3.184	3.687	3.602	2.514	4.134	3.015	2.106	2.367

Equation (12) was applied to the same ten high-performance industrial ejectors, in order to find the corresponding values of the diffuser efficiency η_D. Table 4 also reports the values of the Mach number M_{m-2} calculated using Equation (11), as well as the values of the Mach number M_{m-i} calculated using Equation (17). The values of η_D vs. M_{m-2} are plotted in Figure 7, which also shows the regression line (R^2 = 0.9725).

As mentioned in Section 2.2.2, determining the Mach number M_{m-2} requires prior knowledge of the pressure p_2. To overcome this problem, Equation (17) was used to calculate the Mach number M_{m-i} reached by the motive gas at the outlet of the nozzle with the pressure p_i of the induced gas, as if this were not accelerated in the suction chamber by w_i to w_2 (Figure 1). The resulting diagram (Figure 8) shows that the correlation between the efficiency of the diffuser η_D and the Mach number M_{m-i} was better than the previous one, with a coefficient of determination R^2 equal to 0.9741. Therefore, the relationship found $\eta_D = f(M_{m-i})$, as a result of linear regression, as follows:

$$\eta_D = -0.0609 \cdot M_{m-i} + 0.932 \tag{19}$$

3.2. Validation of the Mathematical Modelling of the Entrainment Ratio vs. the Values of Industrial Ejectors

To validate the results of the mathematical modelling of the industrial entrainment ratio, represented by Equations (18) and (10), it is necessary to compare the calculated entrainment ratios from Equation (10) with those declared by the manufacturer of the ten high performance ejectors (Table 1). This comparison produced an average error only of 1.7%, due to the linear relationship presented in Equation (19), characterized by R^2 = 0.9741 < 1.

3.3. Calculation of the Industrial Entrainment Ratio on Benchmark Ejectors Built and Tested to Use in ERSs

Following the method indicated in Section 2.2.2, Equation (17) allowed for calculation of the Mach Number M_{m-i}. Then, Equation (19) made it possible to calculate the efficiency of the diffuser η_D. Consequently, Equation (18) allowed us to calculate the best pressure p_2, and finally, Equation (10) allowed us to calculate the industrial entrainment ratio ω_{ind}.

This method was applied to each of the benchmark ejectors presented in Tables 2 and 3. The calculation results are shown in Tables 5 and 6, respectively, together with the experimental entrainment ratio value ω_{exp} and the relative percentage difference: $\delta = \frac{\omega_{exp} - \omega_{ind}}{\omega_{ind}} \cdot 100$.

Equations (10), (17) and (18), as well as the auxiliary Equations (14)–(16), contain the quantities k_m, k_i, k_4, R_m, R_i, and R_4. In all ejectors presented in Tables 2 and 3, the induced gas was the same as the motive gas. Therefore, $k_m = k_i = k_4 = k$ and $R_m = R_i = R_4 = R$. Tables 5 and 6 shows the values of the gas constant R calculated for each gas by the following formula:

$$R = \frac{\overline{R}}{m_m}, \tag{20}$$

where m_m is the molecular mass found in [19] and $\overline{R}$ is the universal gas constant equal to 8314 (J kmole^{-1}K^{-1}).

Table 5. Results of mathematical modelling applied to the first series of benchmark ejectors (Table 2), in order to determine the industrial entrainment ratio ω_{ind} vs. the experimental one ω_{exp}.

Test n.	Ref.	Geom. [19]	Case [19]	Run [19]	R	k	c_p (J kg^{-1}K^{-1})	M_{m-i} Mach N.	η_D	p_2 (bar)	ω_{ind}	ω_{exp}	δ (%)
1	[53]	A	1	f	461.8	1.14	3757	3.266	0.733	0.0243	2.011	1.200	−40.3%
2	[54]	M	1	i	461.8	1.14	3757	6.934	0.510	0.0103	0.708	0.400	−43.5%
3	[54]	M	2	e	461.8	1.14	3757	6.767	0.520	0.0101	0.940	0.513	−45.4%
4	[54]	M	3	g	461.8	1.14	3757	7.092	0.500	0.0079	0.551	0.310	−43.8%
5	[55]	B	1	d	72.93	1.125	656	1.771	0.824	1.895	0.289	0.240	−17.0%
6	[55]	B	2	c	72.93	1.125	656	1.630	0.833	2.292	0.449	0.408	−18.2%
7	[56]	C	1	h*	81.5	1.165	575	1.952	0.813	2.855	0.586	0.329	−43.9%
8	[56]	C	1	p*	81.5	1.165	575	1.952	0.813	2.917	0.447	0.252	−43.6%
9	[56]	C	2	d*	81.5	1.165	575	1.903	0.816	3.118	0.618	0.393	−36.4%
10	[56]	C	2	k*	81.5	1.165	575	1.903	0.816	3.170	0.488	0.293	−39.9%
11	[56]	C	3	d*	81.5	1.165	575	1.842	0.820	3.464	0.707	0.489	−30.8%
12	[56]	C	3	h*	81.5	1.165	575	1.842	0.820	3.499	0.574	0.390	−32.1%
13	[56]	C	4	e*	81.5	1.165	575	1.790	0.823	3.786	0.822	0.554	−32.6%
14	[56]	C	4	i*	81.5	1.165	575	1.790	0.823	3.824	0.641	0.438	−31.6%
15	[57]	F	1		81.5	1.165	575	1.786	0.823	3.361	0.990	0.592	−40.2%
16	[57]	F	2		81.5	1.165	575	2.057	0.807	2.794	0.733	0.361	−50.8%
17	[57]	F	3		81.5	1.165	575	1.964	0.812	3.308	1.016	0.433	−57.4%
18	[58]	I	1	c*	81.5	1.165	575	1.908	0.816	3.337	0.816	0.459	−43.8%
19	[58]	I	1	d*	81.5	1.165	575	1.908	0.816	3.346	0.755	0.416	−44.9%
20	[58]	J	1	d	81.5	1.165	575	1.908	0.816	3.345	0.765	0.476	−37.8%
21	[58]	K	1	e	81.5	1.165	575	1.908	0.816	3.352	0.725	0.504	−30.5%
22	[59]	G	1	c	62	1.100	682	2.300	0.792	0.594	0.571	0.310	−45.7%
23	[59]	G	2	c	62	1.100	682	2.219	0.797	0.698	0.651	0.400	−38.6%
24	[59]	G	3	b*	62	1.100	682	2.139	0.802	0.817	0.805	0.550	−31.7%
25	[59]	G	3	c*	62	1.100	682	2.139	0.802	0.820	0.741	0.480	−35.2%
26	[59]	H	1	b*	62	1.100	682	2.300	0.792	0.588	0.654	0.410	−37.3%
27	[59]	H	1	c*	62	1.100	682	2.300	0.792	0.590	0.617	0.340	−44.9%
28	[59]	H	2	b*	62	1.100	682	2.219	0.797	0.691	0.777	0.540	−30.5%
29	[59]	H	2	c*	62	1.100	682	2.219	0.797	0.695	0.702	0.480	−31.6%
30	[59]	H	3	b*	62	1.100	682	2.139	0.802	0.813	0.937	0.680	−27.4%
31	[59]	H	3	c*	62	1.100	682	2.139	0.802	0.817	0.808	0.590	−27.0%
32	[60]	D	1	f*	71.12	1.115	690	2.325	0.790	0.338	0.666	0.247	−62.9%
33	[60]	D	1	g*	71.12	1.115	690	2.325	0.790	0.339	0.643	0.239	−62.8%
34	[60]	D	2	f*	71.12	1.115	690	2.449	0.783	0.267	0.485	0.123	−74.6%
35	[60]	D	2	g*	71.12	1.115	690	2.449	0.783	0.268	0.467	0.116	−75.1%
36	[60]	D	3	f	71.12	1.115	690	2.577	0.775	0.210	0.354	0.063	−82.2%
37	[61]	L	1	f	287	1.4	1005	1.020	0.870	4.456	1.023	0.452	−55.8%

Table 6. Results of mathematical modelling applied to the second series of benchmark ejectors (Table 3), in order to determine the industrial entrainment ratio ω_{ind} vs. the experimental one ω_{exp}.

Test n.	Ref.	Figure of Ref.	Case	Run	R	k	c_p (J kg^{-1}K^{-1})	M_{m-i} Mach N.	η_D	p_2 (bar)	ω_{ind}	ω_{exp}	δ (%)
38	[62]	4a	CON	13.4-D1.4	461.8	1.14	3757	3.647	0.710	0.00803	0.588	0.367	−37.6%
39	[62]	4a	CON	19-D2.0	461.8	1.14	3757	3.647	0.710	0.00803	0.588	0.367	−37.6%
40	[62]	4a	CON	13.4-D1.7	461.8	1.14	3757	3.647	0.710	0.00829	0.449	0.188	−58.1%
41	[62]	4a	CON	19-D2.4	461.8	1.14	3757	3.647	0.710	0.00845	0.388	0.167	−57.1%
42	[62]	4b	CON	D1.4	461.8	1.14	3757	3.647	0.710	0.00803	0.591	0.276	−53.3%
43	[62]	4b	CRMC	D1.4	461.8	1.14	3757	3.647	0.710	0.00800	0.610	0.390	−36.1%
44	[62]	4b	CON	D1.7	461.8	1.14	3757	3.647	0.710	0.00829	0.447	0.190	−57.5%
45	[62]	4b	CRMC	D1.7	461.8	1.14	3757	3.647	0.710	0.00825	0.465	0.267	−42.6%
46	[63]	5	p_m	116	461.8	1.14	3757	3.158	0.740	0.00984	1.627	0.617	−62.1%
47	[63]	5	p_m	153	461.8	1.14	3757	3.285	0.732	0.00972	1.205	0.486	−59.7%
48	[63]	5	p_m	198	461.8	1.14	3757	3.402	0.725	0.00979	0.851	0.389	−54.5%
49	[63]	5	p_m	270	461.8	1.14	3757	3.542	0.716	0.00993	0.709	0.343	−51.6%
50	[63]	6	p_i	1.306	461.8	1.14	3757	3.402	0.725	0.00979	0.848	0.389	−54.0%
51	[63]	6	p_i	1.933	461.8	1.14	3757	3.223	0.736	0.01443	1.313	0.643	−51.0%
52	[63]	6	p_i	2.346	461.8	1.14	3757	3.135	0.741	0.01774	1.704	0.769	−54.9%
53	[64]	9	p_m	350	461.8	1.14	3757	1.722	0.827	0.5761	0.625	0.430	−31.2%
54	[64]	9	p_m	450	461.8	1.14	3757	1.867	0.818	0.5826	0.435	0.324	−25.5%
55	[64]	9	p_m	550	461.8	1.14	3757	1.977	0.812	0.5929	0.333	0.222	−33.3%
56	[64]	10	p_i	90	461.8	1.14	3757	1.722	0.827	0.7391	0.655	0.464	−29.2%
57	[64]	10	p_i	70	461.8	1.14	3757	1.867	0.818	0.5826	0.435	0.324	−25.5%
58	[64]	10	p_i	50	461.8	1.14	3757	2.050	0.807	0.4319	0.265	0.181	−31.8%
59	[65]	3	p_i	90	62	1.100	682	1.850	0.819	0.7698	0.328	0.132	−59.8%
60	[65]	3	p_i	95	62	1.100	682	1.821	0.821	0.8082	0.355	0.152	−57.2%
61	[65]	3	p_i	100	62	1.100	682	1.792	0.823	0.8489	0.384	0.172	−55.2%
62	[65]	3	p_i	105	62	1.100	682	1.764	0.825	0.8879	0.413	0.193	−53.4%
63	[65]	3	p_i	110	62	1.100	682	1.737	0.826	0.9270	0.445	0.213	−52.1%
64	[65]	3	p_i	115	62	1.100	682	1.712	0.828	0.9638	0.478	0.233	−51.2%
65	[65]	3	p_i	120	62	1.100	682	1.687	0.829	1.0035	0.511	0.251	−50.9%
66	[66]	3	p_m	2148	81.5	1.165	575	1.906	0.816	2.4876	1.255	0.626	−50.1%
67	[66]	3	p_m	2340	81.5	1.165	575	1.954	0.813	2.4723	1.023	0.528	−48.4%
68	[66]	3	p_m	2495	81.5	1.165	575	1.989	0.811	2.4663	0.953	0.481	−49.5%

Tables 5 and 6 also show the values of the ratio of specific heat k. As the bibliography provided disparate values, they were calculated as follows: For each group of ejectors characterized by the same gas, the average of the pressures p_m and temperatures T_m (Figure 1 and Tables 2 and 3) and the average of the pressures p_i were calculated, noting that the S.D. was limited. The average value of the pressure p_m and temperature T_m of each gas made it possible to trace the point of the boundary condition m (Figure 1) on the p–h diagram of the gas. Considering the isentropic expansion of the motive gas in the nozzle, the mean value of p_i made it possible to trace, on the p–h diagram, the point of isentropic conditions at the outlet of the nozzle. In correspondence to the two points (m and i) the p–h diagram provided the enthalpy values h_m and $h_{i\text{-}is}$ and, therefore, the isentropic difference in enthalpies $\Delta h_{m-is} = (h_m - h_{i-is})$. As the temperature $T_{m\text{-}is}$ can be read from the p–h diagram, and as $\Delta h_{m-is} = c_p \cdot (T_m - T_{i-is})$, the specific heat at constant pressure c_p can therefore be obtained as follows:

$$c_p = \frac{\Delta h_{m-is}}{(T_m - T_{i-is})}. \tag{21}$$

Meyer's relationship provides the specific heat at constant volume c_v:

$$c_v = c_p - R. \tag{22}$$

Finally, k, the ratio of the two specific heats, is obtained as follows:

$$k = \frac{c_p}{c_v}. \tag{23}$$

After having obtained the best pressure p_2 with the method in Section 2.2.2, Equation (8), with $k_i = k$ and $R_i = R$, provides the value of the isentropic difference in the enthalpies Δh_2. Plotting of the points i and $2is$ on the p–h diagram made it possible to measure the exact value of Δh_2, which was found to be superimposable to the value provided by Equation (8), with an error of less than 2%.

Therefore, the ratio of specific heats k obtained from the expansion of the motive gas was also usable for the expansion of the induced gas and, according to Equations (A1)–(A3), also for the diffusion of the mixed gases.

On the other hand, this method for calculating the specific heat ratio k is the same as that adopted previously [67] to quantify the k of the wet steam result equal to 1.14. It is very different from the value of 1.3 for dry steam, as the specific heat c_p of the wet steam calculated by Equation (21) considers the latent heat released during the partial condensation and which is present in the quantification of $\Delta h_{m-is} = (h_m - h_{i-is})$ by the h–s Mollier diagram.

Differences between the experimental and industrial entrainment ratios presented in Tables 5 and 6 are also depicted in the histograms of Figures 9 and 10, respectively.

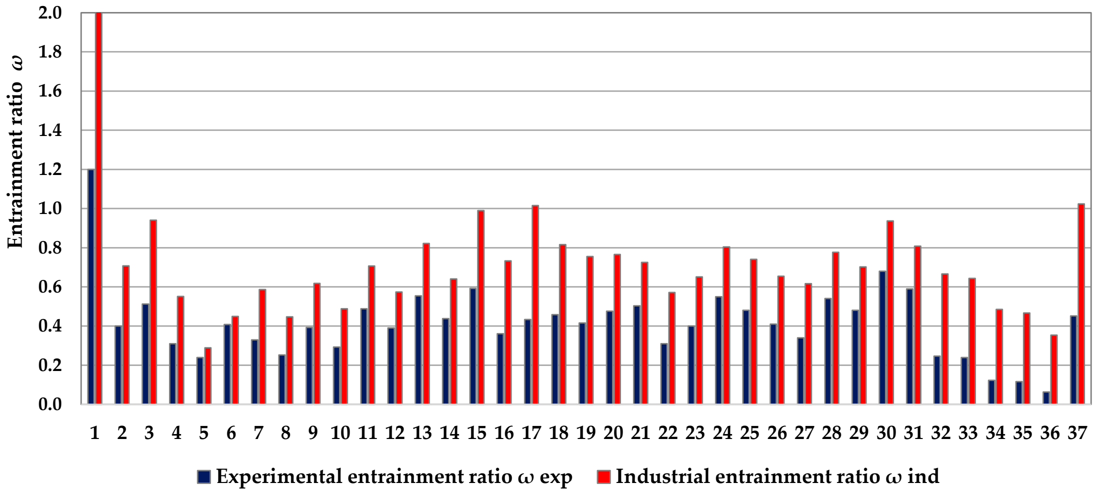

Figure 9. Industrial entrainment ratios ω_{ind} vs. experimental ones ω_{exp} for the first series of benchmark ejectors (Table 5).

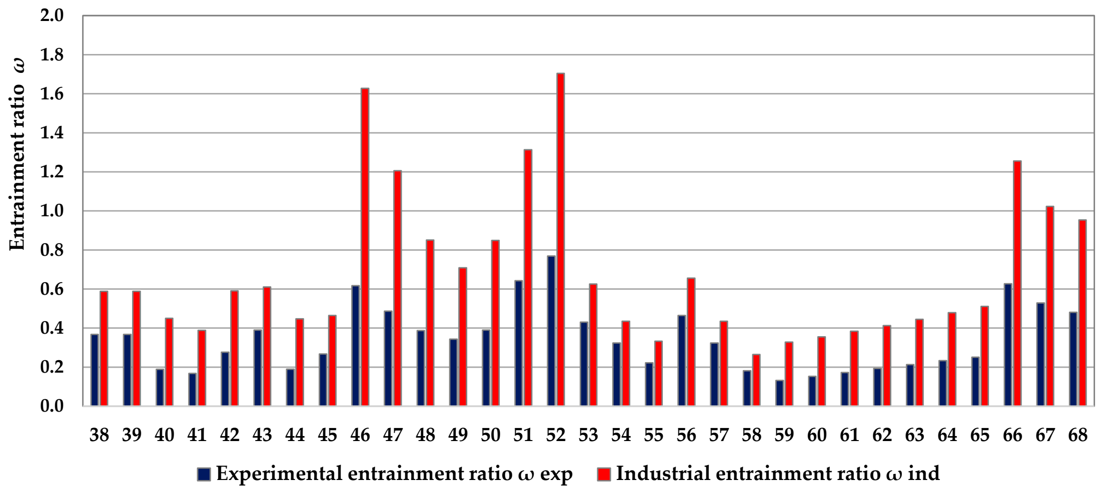

Figure 10. Industrial entrainment ratios ω_{ind} vs. experimental ones ω_{exp} for the second series of benchmark ejectors (Table 6).

4. Discussion and Conclusions

The long experience, extending for over a century, of the manufacturers of ejectors for the chemical, oil, and food industries, has led some of them to improve their products, where improving an ejector means maximizing the entrainment ratio ω. For this reason, these high entrainment ratios are called here: industrial entrainment ratios.

However, Chen, in his 1997 work [63], wrote: "Although ejector manufacturers possess much valuable experimental data, they are understandably reluctant to publish this data". Almost a quarter of a century has passed since then, and Chen's statement is still valid. It is even impossible to know the entrainment ratio values with respect to the boundary conditions unless the ejector is purchased.

The first studies conducted in Germany in the 1930s led to a mathematical model for calculating the entrainment ratio ω based on the momentum theorem and on the identification of isentropic efficiencies of expansion and diffusion. The same German studies showed that it was necessary to accelerate the induced gas before it entered the mixing chamber (Figure 1). The acceleration in the suction chamber—and, therefore, the reduction in the pressure p_2 at the inlet of the mixing chamber—cannot be indiscriminate but should be designed to reduce the speed difference between the motive gas and the induced gas in the mixing chamber, while avoiding an excessive compression ratio in the diffuser which, instead, negatively affects the entrainment ratio ω.

The best value of this acceleration—and, therefore, the best value of the discharge pressure from the suction chamber of the induced gas p_2—is usually determined [68] by searching for the maximum of the function represented by Equation (10), assuming the value of the diffuser efficiency η_D to be constant.

In this work, the diffuser efficiency η_D was instead considered to be variable, depending on the Mach number of the motive gas at the inlet in the mixing chamber.

Therefore, Equation (10) was studied analytically as a function of two variables: p_2 and η_D (Figures 4–6). Two equations were produced as a result: Equation (13), of which the solution provides the best values of p_2 with respect to the industrial entrainment ratio ω_{ind}, and Equation (12), which provides the efficiency of the diffuser η_D always with respect to the industrial entrainment ratio ω_{ind}.

If the entrainment ratio ω_{ind} inserted into Equations (13) and (12) is that of a high-performance ejector, such as those produced by the most competitive manufacturers mentioned at the beginning of this discussion, then Equation (13) gives the relative value of p_2 and Equation (12) provides the efficiency of the diffuser η_D of this ejector.

This calculation method was applied to ten high-performance industrial ejectors from a major European company, which has operated in the global ejector market for eighty years. This choice was made in order to have a heterogeneous population of boundary conditions (i.e., p_m, p_i, and p_4). To circumvent the problem of scarce data availability for industrial ejectors, as stated by Chen [63], a manufacturer of evaporators for the food industry was asked to make available their data archive of the ejectors purchased over the course of twenty years from a big European company.

For each ejector, in addition to p_2 and η_D, the Mach number of the motive gas M_{m-i} was also calculated, using Equation (17). Comparison between the efficiency of the diffuser η_D and the Mach number M_{m-i} produced Equation (19), which is a linear regression function characterized by a high coefficient of determination R^2, confirming that the hypothesis $\eta_D = f(M_{m-i})$ is consistent.

In the second part of the present work, comprising mathematical modelling, from Equation (10), the function (18) was obtained, of which the solution gives the value of the pressure p_2 which maximizes the entrainment ratio. Equation (18) contains the quantity η_D which depends, through Equation (19), on the Mach Number M_{m-i} which, in turn, according to Equation (17), is only dependent on the known boundary conditions p_m and p_i. Finally, Equation (10) can provide the maximized value of entrainment ratio, that is industrial entrainment ratio ω_{ind}.

This procedure was applied to a series of 68 ejectors built and tested experimentally over the last twenty years or so (Tables 2 and 3), as a part of research activities aimed at developing heat-driven ejector refrigeration systems (ERSs); for this reason, they were called benchmark ejectors [19]. The renewed interest in this type of refrigeration system, mainly due to environmental concerns (as they can operate on solar energy), has activated the interest of many researchers towards the study of the functioning of supersonic ejectors through computational methods. Such numerical investigations have produced more and more refined results, are now able to simulate the functioning of the ejectors and to predict, with relative precision, the experimental entrainment ratios ω_{exp} [19] of the benchmark ejectors.

Again, with reference to the second part of this work, the results of the procedure for calculating the industrial entrainment ratio ω_{ind}, applied to the series of 68 benchmark ejectors, are presented in Tables 5 and 6 (as well as in Figures 9 and 10), where they were compared with the experimental entrainment ratio values ω_{exp}.

The experimental entrainment ratios ω_{exp} were always lower than the industrial ones ω_{ind}, with a minimum difference of -17% for the ejector of [55] and a maximum difference of about -80% for the ejector of [60]. Limited differences of about -30% were also found for the ejectors of [56,58,59] and only -25% for the ejector of [64]. For many other ejectors, the differences were consistent. This means that, while numerical analysis in this field has shown promise, it must be extended to the search for the best geometry of the ejector elements, first ensuring that the suction chamber has an outlet section which provides the best pressure p_2, to be obtained a priori, for example, using the analytical method proposed herein. Second, it is necessary to pay close attention to the shape and size of the mixing chamber, wherein the shock train phenomena are very complex. Therefore, researchers who have the objective of designing a high-performance ejector should repeat the numerical analysis, which has only a checking character, with simulated variations in the shape and size of the mixing chamber, in an attempt to reach the high value of the entrainment ratio of industrial ejector. The industrial value can be calculated, for example, using the method proposed in this work, and corresponds to those of high-performance ejectors already on the market.

Finally, Equation (19) proposed in this work, which indicates the influence of the Mach number of motive gas at the inlet of mixing chamber M_{m-i} on the diffuser efficiency η_D with good precision, allows for calculation of the latter in the extreme situations encountered during the survey on 68 laboratory ejectors (Tables 5 and 6). These are the ejectors [61] with a minimum Mach number M_{m-i} of about 1, for which Equation (19) proposes a diffuser efficiency η_D of 0.870 and, excluding the ejector of [54], the ejector of [62] with the relative maximum M_{m-i} of almost four, for which the diffuser efficiency η_D is 0.710. It must be remembered that, in this work, the diffuser efficiency η_D takes into account the whole loss during the pressure gain process due to shock train and subsonic diffuser section and, as a unitary mixing efficiency was assumed in Equation (1), any energy losses during mixing are also represented by η_D, due to the adopted mode of calculation of η_D.

Furthermore, study of the partial derivative of Equation (10) shows an average value of $\frac{\partial\omega}{\partial\eta_D} = 2.1 \pm 0.1$. If a constant diffuser efficiency η_D had been chosen, for example, equal to 0.770, as indicated by [68] (or 0.807, as indicated by [16,23]), in the ejector of [61], the absolute error in the maximum entrainment ratio prediction ω_{ind} would have been $\Delta\omega = \frac{\partial\omega}{\partial\Delta\eta_D}\cdot\Delta\eta_D = 2.1\cdot(0.770 - 0.870) = -0.21$, corresponding to a relative error of $\Delta\omega\% = \frac{\Delta\omega}{\omega_{top}}\cdot 100 = \frac{0.21}{1.02}\cdot 100 = -20.5\%$. Similarly, the case of the ejector of [62], the absolute error is $\Delta\omega = \frac{\partial\omega}{\partial\eta_D}\cdot\Delta\eta_D = 2.1\cdot(0.770 - 0.710) = 0.126$, corresponding to a relative error of $\Delta\omega\% = \frac{\Delta\omega}{\omega_{top}}\cdot 100 = \frac{0.126}{0.588}\cdot 100 = 21.4\%$. Therefore, Equation (19) allows the elimination of relative errors in the ω_{ind} prediction between about $\pm 20\%$. The next step will be to expand the sample of industrial ejectors, especially towards the high values of the Mach number, in order to verify Equation (19) even in cases such as the (rare) one of [54], with M_{m-i} equal to about 7.

In conclusion, it is useful to say that in this work, the objective was not for the design method of ejectors to have the optimal entrainment ratio, but rather for an algorithm to determine the maximum value of the entrainment ratio, built through the application of Calculus [69–71]. This algorithm can be used to determine the maximum (therefore optimal) value of the entrainment ratio ω of the ejector operating at the expected boundary conditions represented by the pressures and temperatures of the motive gas (p_m, T_m), of the induced gas (p_i, T_i), and of the pressure of the mixed gases (p_4). The maximum values, therefore optimal, of entrainment ratios obtained with the algorithm are those (ω_{ind}) corresponding to the industrial ejectors of the big European manufacturer chosen because it is the one with the longest experimental research history and with the greatest diffusion in the world market of ejectors.

Starting from the best value of entrainment ratio $\omega = \omega_{ind}$, obtainable with the algorithm of this work, the researchers with experience in CFD applied to ejectors, will have to use the computational methods repeatedly, varying the dimensions especially of the mixing chamber, until the CFD provides the value of the entrainment ratio equal to ω_{ind}. This is a similar method adopted in machine design with the FEA [72].

Funding: This research received no external funding.

Institutional Review Board Statement: Not applicable.

Informed Consent Statement: Not applicable.

Data Availability Statement: The data presented in this study are contained within the article.

Acknowledgments: Roberto Stivanello, technician of Food Processes Engineering Laboratory, for his contribution during the tests on the industrial ejectors.

Conflicts of Interest: The author declares no conflict of interest.

Nomenclature

Symbol	**Quantity**
c_p	specific heat at constant pressure
c_v	specific heat at constant volume
D_i	intake pipe diameter of the induced gas
D_4	exit pipe diameter of the mixed gases
G_m	mass flow rate of the motive gas
G_i	mass flow rate of the induced gas
k_m	ratio of specific heats c_p/c_v of the motive gas
k_i	ratio of specific heats c_p/c_v of the induced gas
k_4	ratio of specific heats c_p/c_v of the mixed gases
M_{m-2}	Mach number of the motive gas at the nozzle exit when pressure is $p_1 = p_2$
$M_{m-\mathrm{i}}$	Mach number of the motive gas at the nozzle exit when pressure is $p_1 = p_i$
p_m	pressure of the motive gas at the inlet of the nozzle
p_i	pressure of the induced gas at the inlet of the suction chamber
p_1	pressure of the motive gas at the nozzle exit
p_2	pressure of the induced gas at the exit of the suction chamber, equal to p_1
p_3	pressure of the mixed gas at the end of mixing chamber, equal to p_2
p_4	pressure of the mixed gases at the exit of the diffuser
R_m	specific constant of the motive gas
R_i	specific constant of the induced gas
R_4	specific constant of the mixed gases
T_m	absolute stagnation temperature (K) of the motive gas
t_m	stagnation temperature (°C) of the motive gas
T_i	absolute stagnation temperature (K) of the induced gas
T_4	absolute stagnation temperature (K) of the mixed gases
w_1	supersonic velocity of the motive gas at the inlet of mixing chamber

w_2	subsonic velocity of the induced gas at the inlet of mixing chamber
w_3	velocity of the mixed gases in the mixing chamber
w_m	velocity of the motive gas at the inlet of the nozzle
w_i	velocity of the induced gas at the inlet of the suction chamber
w_4	velocity of the mixed gases at the exit of the diffusor
Greek symbol	Quantity
Δh_1	isentropic difference in enthalpies of the motive stream in the nozzle
Δh_2	isentropic difference in enthalpies of the induced stream in the suction chamber
Δh_3	isentropic difference in enthalpies of the mixed stream in the diffusion
η_{E1}	isentropic efficiency in the nozzle
η_{E2}	isentropic efficiency in the suction chamber
η_D	isentropic efficiency of the diffusion
ω	Entrainment ratio (G_i/G_m)
ω_{ind}	Entrainment ratio of the industrial ejectors (therefore optimal)
ω_{exp}	Entrainment ratio of the experimental laboratory ejectors designed by CFD

Appendix A

The specific heat at constant pressure of the mixed gases, c_{p4}, is dependent on the specific heat of motive gas, c_{pm}, of the specific heat of induced gas, c_{pi}, and of the entrainment ratio ω:

$$c_{p4} = \frac{c_{pm} + \omega \cdot c_{pi}}{1+\omega} \tag{A1}$$

Similarly, the specific heat at constant volume of the mixed gases, c_{v4}, is as follows:

$$c_{v4} = \frac{c_{vm} + \omega \cdot c_{vi}}{1+\omega} \tag{A2}$$

Hence, the specific heat ratio of the mixed gases, k_4, is as follows:

$$k_4 = \frac{c_{v4}}{c_{p4}}. \tag{A3}$$

The specific gas constant of mixed gases, R_4, is given by the following:

$$R_4 = c_{p4} - c_{v4}. \tag{A4}$$

Finally, due to enthalpy balance, the absolute stagnation temperature of the mixed fluid, T_4, is as follows:

$$T_4 = \frac{c_{pm} \cdot T_m + \omega \cdot c_{pi} \cdot T_i}{c_{pm} + \omega \cdot c_{pi}}. \tag{A5}$$

References

1. Power, R.B. *Steam Jet Ejector for the Process Industries*, 1st ed.; Mac Graw-Hill: New York, NY, USA, 1994; pp. 7–18.
2. Matsuo, K.; Miyazato, Y.; Kim, H.D. Shock train and pseudo-shock phenomena in internal gas flows. *Prog. Aerosp. Sci.* **1999**, *35*, 33–100. [CrossRef]
3. Thevenot, R. *Histoire du Froid Artificiel*, 1st ed.; Institut International du Froid: Paris, France, 1978; pp. 63–64.
4. Pollerberg, C.; Heinzel, A.; Weidner, E. Model of a solar driven steam jet ejector chiller and investigation of its dynamic operational behaviour. *Sol. Energy* **2009**, *83*, 732–742. [CrossRef]
5. Keenan, J.H.; Neumann, E.P. A simple air ejector. *ASME J. Appl. Mech.* **1942**, *9*, A75–A81. [CrossRef]
6. Keenan, J.H.; Neumann, E.P.; Lustwerk, F. An investigation of ejector design by analysis and experiment. *ASME J. Appl. Mech.* **1950**, *17*, 299–309. [CrossRef]
7. Lukasiewicz, J. Diffusers for supersonic wind tunnels. *J. Aeronaut. Sci.* **1953**, *20*, 617–626. [CrossRef]
8. Shapiro, A.H. *The Dynamics and Thermodynamics of Compressible Fluid Flow*, 1st ed.; Ronald Press: New York, NY, USA, 1953; Volume 1, pp. 99, 135–139, 152.
9. Nill, L.D.; Mattick, A.T. An experimental study of shock structure in a normal shock train. In Proceedings of the AIAA 34th Aerospace Sciences Meeting and Exhibit, Reno, NV, USA, 15–18 January 1996; p. 96-0799. [CrossRef]
10. McCormick, D.C. Shock boundary-layer interaction control with vortex generators and passive cavity. *AIAA J.* **1993**, *31*, 91–96. [CrossRef]

11. Sullins, G.; McLafferty, G. Experimental results of shock trains in rectangular ducts. In Proceedings of the AIAA 4th International Aerospace Planes Conference, Orlando, FL, USA, 1–4 December 1992; p. 92-5103. [CrossRef]
12. Carroll, B.F.; Dutton, J.C. Multiple normal shock wave/turbulent boundary-layer interactions. *J. Propuls. Power* **1992**, *8*, 441–448. [CrossRef]
13. Lin, P.; Rao, G.V.R.; O'Connor, G.M. Numerical analysis of normal shock train in a constant area isolator. In Proceedings of the AIAA 27th Joint Propulsion Conference, Sacramento, CA, USA, 24–26 June 1991; p. 91-2162. [CrossRef]
14. Sajben, M.; Donovan, J.F.; Morris, M.J. Experimental investigation of terminal shock sensors for mixed-compression inlets. *J. Propuls. Power* **1992**, *8*, 168–174. [CrossRef]
15. Munday, J.T.; Bagster, D.F. A new ejector theory applied to steam jet refrigeration. *Ind. Eng. Chem. Process Des. Dev.* **1977**, *16*, 442–449. [CrossRef]
16. Eames, I.W.; Aphornaratana, S.; Haider, H. A theoretical and experimental study of a smallscale steam jet refrigerator. *Int. J. Refrig.* **1995**, *18*, 378–385. [CrossRef]
17. Huang, B.J.; Chang, J.M.; Wang, C.P.; Petrenko, V.A. A 1-D analysis of ejector performance. *Int. J. Refrig.* **1999**, *18*, 354–364. [CrossRef]
18. Rogdakis, E.D.; Alexis, G.K. Investigation of ejector design at optimum operating condition. *Energy Convers. Manag.* **2000**, *41*, 1841–1849. [CrossRef]
19. Besagni, G.; Cristiani, N.; Croci, L.; Guedon, G.R.; Inzoli, F. Computational fluid-dynamics modelling of supersonic ejectors: Screening of modelling approaches, comprehensive validation and assessment of ejector component efficiencies. *Appl. Therm. Eng.* **2021**, *186*, 116431. [CrossRef]
20. Rusly, E.; Aye, L.; Charters, W.W.S.; Ooi, A. CFD analysis of ejector in a combined ejector cooling system. *Int. J. Refrig.* **2005**, *28*, 1092–1101. [CrossRef]
21. Pianthong, K.; Seehanam, W.; Behnia, M.; Sriveerakul, T.; Aphornratana, S. Investigation and improvement of ejector refrigeration system using computational fluid dynamics technique. *Energy Convers. Manag.* **2007**, *48*, 2556–2564. [CrossRef]
22. Zhu, Y.; Cai, W.; Wen, C.; Li, Y. Numerical investigation of geometry parameters for design of high-performance ejectors. *Appl. Therm. Eng.* **2009**, *29*, 898–905. [CrossRef]
23. Varga, S.; Oliveira, A.C.; Diaconu, B. Numerical assessment of steam ejector efficiencies using CFD. *Int. J. Refrig.* **2009**, *32*, 1203–1211. [CrossRef]
24. Varga, S.; Oliveira, A.C.; Ma, X.; Omer, S.A.; Zhang, W.; Riffat, S.B. Comparison of CFD and experimental performance results of a variable area ratio steam ejector. *Int. J. Low-Carbon Technol.* **2010**, *6*, 119–124. [CrossRef]
25. Ji, M.; Utomo, T.; Woo, J.; Lee, Y.; Jeong, H.; Chung, H. CFD investigation on the flow structure inside thermo vapor compressor. *Energy* **2010**, *35*, 2694–2702. [CrossRef]
26. Wang, X.D.; Dong, J.L. Numerical study on the performances of steam-jet vacuum pump at different operating conditions. *Vacuum* **2010**, *84*, 1341–1346. [CrossRef]
27. Yang, X.; Long, X.; Yao, X. Numerical investigation on the mixing process in a steam ejector with different nozzle structures. *Int. J. Therm. Sci.* **2012**, *56*, 95–106. [CrossRef]
28. Yazdani, M.; Alahyari, A.A.; Radcliff, T.D. Numerical modeling of two-phase supersonic ejectors for work-recovery applications. *Int. J. Heat Mass Transf.* **2012**, *55*, 5744–5753. [CrossRef]
29. Sharifi, N.; Boroomand, M. An investigation of thermo-compressor design by analysis and experiment: Part 1. Validation of the numerical method. *Energy Convers. Manag.* **2013**, *69*, 217–227. [CrossRef]
30. Wang, X.; Dong, J.; Li, A.; Lei, H.; Tu, J. Numerical study of primary steam superheating effects on steam ejector flow and its pumping performance. *Energy* **2014**, *78*, 205–211. [CrossRef]
31. Gagan, J.; Smierciew, K.; Butrymowicz, D.; Karwacki, J. Comparative study of turbulence models in application to gas ejectors. *Int. J. Therm. Sci.* **2014**, *78*, 9–15. [CrossRef]
32. Zhu, Y.; Jiang, P. Experimental and numerical investigation of the effect of shock wave characteristics on the ejector performance. *Int. J. Refrig.* **2014**, *40*, 31–42. [CrossRef]
33. Chandra, V.V.; Ahmed, M.R. Experimental and computational studies on a steam jet refrigeration system with constant area and variable area ejectors. *Energy Convers. Manag.* **2014**, *79*, 377–386. [CrossRef]
34. Banasiak, K.; Palacz, M.; Hafner, A.; Bulinski, Z.; Smołka, J.; Nowak, A.J.; Fic, A. A CFD-based investigation of the energy performance of two-phase R744 ejectors to recover the expansion work in refrigeration systems: An irreversibility analysis. *Int. J. Refrig.* **2014**, *40*, 328–337. [CrossRef]
35. Rao, S.; Gopalan, J. Observations on the non-mixed length and unsteady shock motion in a two dimensional supersonic ejector. *Phys. Fluids* **2014**, *26*, 036103. [CrossRef]
36. Arun, K.M.; Tiwari, S.; Mani, A. Three-dimensional numerical investigations on rectangular cross-section ejector. *Int. J. Therm. Sci.* **2017**, *122*, 257–265. [CrossRef]
37. Kong, F.; Kim, H.D. Analytical and computational studies on the performance of a two-stage ejector–diffuser system. *Int. J. Heat Mass Transf.* **2015**, *85*, 71–87. [CrossRef]
38. Besagni, G.; Inzoli, F. Computational fluid-dynamics modeling of supersonic ejectors: Screening of turbulence modeling approaches. *Appl. Therm. Eng.* **2017**, *117*, 122–144. [CrossRef]

39. Varga, S.; Soares, J.; Lima, R.; Oliveira, A.C. On the selection of a turbulence model for the simulation of steam ejectors using CFD. *Int. J. Low-Carbon Technol.* **2017**, *12*, 233–243. [CrossRef]
40. Mazzelli, F.; Giacomelli, F.; Milazzo, A. CFD modeling of condensing steam ejectors: Comparison with an experimental test-case. *Int. J. Therm. Sci.* **2018**, *127*, 7–18. [CrossRef]
41. Haghparast, P.; Sorin, M.V.; Nesreddine, H. The impact of internal ejector working characteristics and geometry on the performance of a refrigeration cycle. *Energy* **2018**, *162*, 728–743. [CrossRef]
42. Thongtip, T.; Aphornratana, S. Development and performance of a heat driven R141b ejector air conditioner: Application in hot climate country. *Energy* **2018**, *160*, 556–572. [CrossRef]
43. Ramesh, A.S.; Sekhar, S.J. Experimental and numerical investigations on the effect of suction chamber angle and nozzle exit position of a steam-jet ejector. *Energy* **2018**, *164*, 1097–1113. [CrossRef]
44. Smierciew, K.; Gagan, J.; Butrymowicz, D. Application of numerical modelling for design and improvement of performance of gas ejector. *Appl. Therm. Eng.* **2019**, *149*, 85–93. [CrossRef]
45. Mohamed, S.; Shatilla, Y.; Zhang, T. CFD-based design and simulation of hydrocarbon ejector for cooling. *Energy* **2019**, *167*, 346–358. [CrossRef]
46. Atmaca, M.; Ezgi, C. Three-dimensional CFD modeling of a steam ejector, Energy Sources, Part A: Recovery. *Utilizat. Environ. Effects* **2019**, 201223538. [CrossRef]
47. Wiegand, J. *Bemessung von Dampfstrahl-Verdichtern und ihr Verhalten bei Wechselnden Betriebsbedingungen*; VDI-Forschungsheft, VDI-Verlag: Berlin, Germany, 1940; Volume 401, pp. 1–24.
48. Grazzini, G.; Milazzo, A.; Mazzelli, F. *Ejectors for Efficient Refrigeration: Design. Applications and Computational Fluid Dynamics*, 1st ed.; Springer: Cham, Switzerland, 2018. [CrossRef]
49. Bosnjakovic, F. *Dampfbefeuchtung in Strahlgebläsen*; VDI-Forschungsheft, VDI-Verlag: Berlin, Germany, 1940; Volume 11, pp. 210–215.
50. Bosnjakovic, F. Über dampfstrahlgebläse. *Zeitschr. Ges. Kälteindustrie* **1936**, *43*, 229–233.
51. Weydanz, W. Die vorgänge in strahlapparaten. *Beiheft Z. Zeitschr. Ges. Kälteindustrie* **1939**, *Reihe 2*, H.8.
52. Grazzini, G.; Mariani, A. A simple program to design a multi-stage jet-pump for refrigeration cycles. *Energy Convers. Manag.* **1998**, *39*, 1827–1834. [CrossRef]
53. Han, Y.; Wang, X.; Sun, H.; Zhang, G.; Guo, L.; Tu, J. CFD simulation on the boundary layer separation in the steam ejector and its influence on the pumping performance. *Energy* **2019**, *167*, 469–483. [CrossRef]
54. Sriveerakul, T.; Aphornratana, S.; Chunnanond, K. Performance prediction of steam ejector using computational fluid dynamics: Part 1. Validation of the CFD results. *Int. J. Therm. Sci.* **2007**, *46*, 812–822. [CrossRef]
55. Gagan, J.; Smierciew, K.; Butrymowicz, D. Performance of ejection refrigeration system operating with R-1234ze(E) driven by ultra-low grade heat source. *Int. J. Refrig.* **2018**, *8*, 458–471. [CrossRef]
56. Poirier, M.; Giguère, D.; Sapoundjiev, H. Experimental parametric investigation of vapor ejector for refrigeration applications. *Energy* **2018**, *162*, 1287–1300. [CrossRef]
57. García Del Valle, J.; Sierra-Pallares, J.; Garcia Carrascal, P.; Castro Ruiz, F. An experimental and computational study of the flow pattern in a refrigerant ejector. Validation of turbulence models and real-gas effects. *Appl. Therm. Eng.* **2015**, *89*, 795–811. [CrossRef]
58. García Del Valle, J.; Saíz Jabardo, J.M.; Castro Ruiz, F.; San José Alonso, J.F. An experimental investigation of a R-134a ejector refrigeration system. *Int. J. Refrig.* **2014**, *46*, 105–113. [CrossRef]
59. Shestopalov, K.O.; Huang, B.J.; Petrenko, V.O.; Volovyk, O.S. Investigation of an experimental ejector refrigeration machine operating with refrigerant R245fa at design and off-design working conditions. Part 2. Theoretical and experimental results. *Int. J. Refrig.* **2015**, *55*, 212–223. [CrossRef]
60. Thongtip, T.; Aphornratana, S. An experimental analysis of the impact of primary nozzle geometries on the ejector performance used in R141b ejector refrigerator. *Appl. Therm. Eng.* **2017**, *110*, 89–101. [CrossRef]
61. Chong, D.; Hu, M.; Chen, W.; Wang, J.; Liu, J.; Yan, J. Experimental and numerical analysis of supersonic air ejector. *Appl. Energy* **2014**, *130*, 679–684. [CrossRef]
62. Kitrattana, B.; Aphornratana, S.; Thongtip, T.; Ruangtrakoon, N. Comparison of traditional and CRMC ejector performance used in a steam ejector refrigeration. *Energy Procedia* **2017**, *138*, 476–481. [CrossRef]
63. Chen, Y.-M.; Sun, C.-Y. Experimental study of the performance characteristics of a steam-ejector refrigeration system. *Exp. Therm. Fluid Sci.* **1997**, *15*, 384–394. [CrossRef]
64. Reddick, C.; Sorin, M.; Sapoundjiev, H.; Aidoun, Z. Effect of a mixture of carbon dioxide and steam on ejector performance: An experimental parametric investigation. *Exp. Therm. Fluid Sci.* **2018**, *92*, 353–365. [CrossRef]
65. Hamzaoui, M.; Nesreddine, H.; Aidoun, Z.; Balistrou, M. Experimental study of a low grade heat driven ejector cooling system using the working fluid R245fa. *Int. J. Refrig.* **2018**, *86*, 388–400. [CrossRef]
66. Yan, J.; Chen, G.; Liu, C.; Tang, L.; Chen, Q. Experimental investigations on a R134a ejector applied in a refrigeration system. *Appl. Therm. Eng.* **2017**, *110*, 1061–1065. [CrossRef]
67. Chaussin, C.; Hilly, G. *Chaleur et Thermodynamique*, 4th ed.; Dunod: Paris, France, 1962; pp. 135–136.
68. Paliwoda, A. Design of supersonic ejectors operating as booster compressor in refrigerating systems. In Proceedings of the XIth International Congress of Refrigeration Science and Technology, Munich, Germany, 31 August 1963; 1965; pp. 589–598. [CrossRef]

69. Friso, D. An approximate analytic solution to a non-Linear ODE for air jet velocity decay through tree crops using piecewise linear emulations and rectangle functions. *Appl. Sci.* **2019**, *9*, 5440. [CrossRef]
70. Friso, D. Conveyor-belt dryers with tangential flow for food drying: Development of drying ODEs useful to design and process adjustment. *Inventions* **2021**, *6*, 6. [CrossRef]
71. Friso, D. Mathematical modelling of conveyor-belt dryers with tangential flow for food drying up to final moisture content below the critical value. *Inventions* **2021**, *6*, 43. [CrossRef]
72. Gu, Z.; Chen, M.; Wang, C.; Zhuang, W. Static and dynamic analysis of a 6300 KN cold orbital forging machine. *Processes* **2021**, *9*, 7. [CrossRef]